

We are IntechOpen, the world's leading publisher of Open Access books Built by scientists, for scientists

6,900

Open access books available

186,000

International authors and editors

200M

Downloads

Our authors are among the

154

Countries delivered to

TOP 1%

most cited scientists

12.2%

Contributors from top 500 universities



WEB OF SCIENCE™

Selection of our books indexed in the Book Citation Index
in Web of Science™ Core Collection (BKCI)

Interested in publishing with us?
Contact book.department@intechopen.com

Numbers displayed above are based on latest data collected.
For more information visit www.intechopen.com



Homology Modeling of Tubulin Isotypes to Investigate MT-Tau Interactions

Vishwambhar Vishnu Bhandare

Abstract

The Homology modeling techniques uses the template structure(s) to model the full-length structure of unknown sequence. It is being used for determining the structure of biological macromolecules, especially proteins. The wide applications of homology modeling approach have helped us to address various challenging problems in the field of biological sciences and drug discovery despite the limitations in using analytical techniques like X-ray, NMR and CryoEM techniques. Here, this chapter emphasize on application of homology modeling in determining MT-Tau interactions which are important in the Alzheimer disease. In Alzheimer diseases, tau detaches from MTs in misfolded shape and forms insoluble aggregates in neurons due to post-translational modifications. MT-tau interactions are largely unknown due to differential expression of neuronal specific tubulin isotypes and intrinsically disordered nature of tau. MTs play crucial roles in important cellular functions including cell division, transport of vesicles, cell signaling, cell motility etc. MTs are composed of different tubulin isotypes which differs mainly at C-terminal tail. In humans, nine β -tubulin isotypes have been reported which are expressed differently in different tissues. Structures for different tubulin isotypes are still lacking due to their complex differential expression pattern and purification. Hence, homology modeling approach allowed us to generate homology models for different neuronal specific tubulin isotypes and study their interactions with tau repeats. It is believed that this study would gain more structural and functional insights to the linked Alzheimer diseases.

Keywords: homology modeling, microtubule, tubulin isotypes, Alzheimer disease, molecular modeling

1. Introduction

Bioinformatics is an interdisciplinary science that uses both computational and informational approaches to retrieve, analyze, organize, visualize, store and develop biological data [1]. It is widely applied in the field of life sciences, especially in functional genomics, sequence analysis, proteomics, drug discovery, etc. Prediction of the structure and functions of the genes and proteins have become a fundamental task in the life science researches. The present book chapter involves molecular modeling study to investigate intermolecular interactions between Microtubule (MT) and Tau. Though these interactions are important in Alzheimer's disease, the

detailed knowledge on MT-Tau interactions are still lacking mainly because of two reasons (i) Lack of full-length structure of tau due to its intrinsically disordered nature and (ii) Differential expression of tubulin isoforms in different type of cells in particular brain and neuronal cells. Earlier experimental efforts have been made to elucidate these interactions using solution structure (PDB ID: 2MZ7.pdb) however correct binding mode and atomistic interactions at structural level are poorly understood. Therefore, this chapter focuses on application of molecular modeling techniques in understanding important MT-Tau interactions in the Alzheimers disease. Bioinformatics approaches like sequence analysis, homology modeling, MD simulations and binding energy calculations are employed systematically to address this challenging problem in the field of Alzheimer's disease.

Tau is intrinsically disordered protein encoded by '*mapt*' gene located on chromosome 17 [2]. The primary function of the tau protein is to bind and stabilize the microtubule. It is abundantly expressed in the brain and neuronal tissues hence its misregulation is associated with the Alzheimers and other neurodegenerative disorders [3, 4]. Till date about six isoforms of tau are reported in the human central nervous system. The length of these six isoforms varies between 352 to 441 residues [5].

Primary structure of tau contains the projectile domain at N-terminal (residue 1–244) which is composed of the acidic and proline-rich region, and the C-terminal repeat domain which consists of 4 repeats i.e., R1, R2, R3 and R4 (residues 245–441) (**Figure 1**). The six isoforms of tau mainly differs by the existence of either R3 or R4 repeats at the C-terminal domain [6]. The one of the tau isoforms is referred as longest isoform mostly observed in humans which comprises 4 repeats i.e., R1, R2, R3 and R4. while the shortest isoform of tau has only 3 repeats (R1, R2 and R3). This shortest isoform of tau is reported in the fetus brain and less common in adults [5, 7]. **Figure 1A** represents the structure of tau repeat region R2 which is bound to the MT composed of $\beta/\alpha/\beta$ tubulin subunits [8]. Hereafter, tau repeat R2 will be mentioned as 'TauR2' for the simplicity. The tau repeats R1, R2, R3 and R4 prefers to bind at the outer surface of microtubule (MT) to stabilize it (**Figure 1A**) and regulates MT polymerization [6]. **Figure 1B** represents domain organization in the tau primary structure and **Figure 1C** shows the sequence of TauR2 which is reported in the CryoEM model. It is well established that tau primarily helps in the assembly and stabilization of axonal MTs, which contributes to the proper functioning of neuronal cells [9]. However, recent studies have reported new functional role of the tau in addition to the axonal, i.e. labile domain of the MT to promote its assembly [10]. Tau detaches from the MTs and forms abnormal, fibrillar structures of insoluble aggregates due to post-translational modifications in Alzheimer diseases and other neurodegenerative diseases associated with tau [11, 12].

Full-length structure of tau protein is not yet determined using X-ray crystallographic techniques due to its intrinsically disordered nature. Also, the efforts to find its solution structure using NMR spectroscopy have failed [13]. Thus, the MT-Tau interactions have been studied so far using various biochemical and biophysical techniques [14–17]. The CryoEM have showed marginal success in determining the structure of tau repeat R2 bound to MT however it shows discontinues density of tau repeats along with each protofilament upon MT binding [8]. Hence, they synthetically developed R1 and R2 repeat of tau and their interactions with MT were examined. These two tau repeats adopts the extended conformation along the crest of protofilament which stabilizes the MT structure by binding to the interface of tubulin dimers [8].

MTs are made from $\alpha\beta$ -tubulin heterodimer subunits [18]. In human, seven α -tubulin and nine β -tubulin isoforms are reported showing their tissue-specific expressions. For instance, β I tubulin isoform is ubiquitously expressed in all cells,

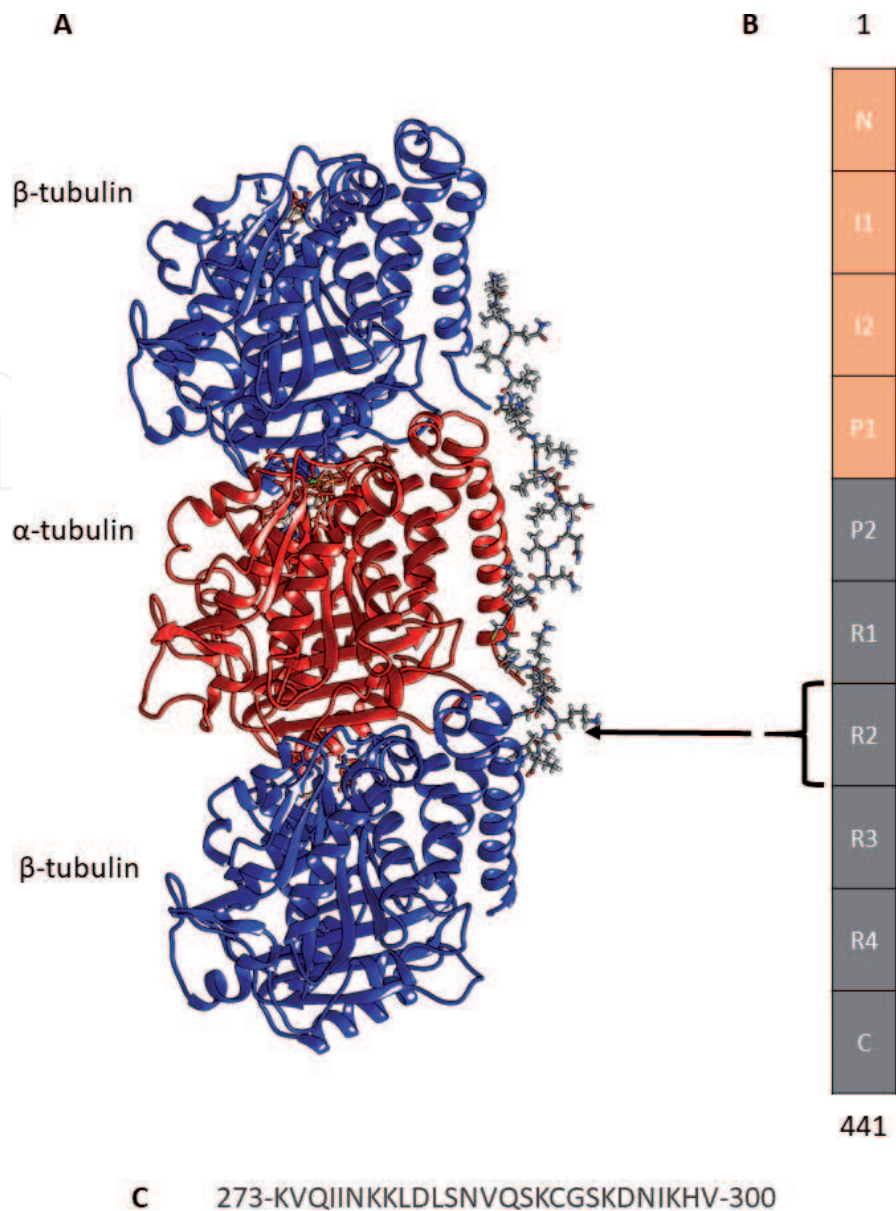


Figure 1. CryoEM Structure of tubulin subunits bound to TauR2. (A) tubulin subunits bound to TauR2 in CryoEM structure 6CVN.pdb. TauR2 domain binds at the outer surface of the MT. (B) Domain organization in tau, (C) sequence of TauR2. [Source: Bhandare et al, 2019; doi: 10.1038/s41598-019-47249-7].

β II and β III tubulin isotype are mainly expressed in brain and neuronal cells, and β VI tubulin isotype is expressed in erythroid cells and platelets [19]. The β I tubulin isotype reported to play crucial role in cell viability, β II tubulin isotype is important for neurite growth and β III tubulin isotype protects nerve cell against free radicals and reactive oxygen species [20]. It has been well known that all β -tubulin isotypes share a significant residue conservation except the C-terminal tail region of MT [21–24] which is flexible in nature and structurally disordered. The C- tail region of all these isotypes overhang outwards of the MTs. The C-tail shows interactions with various MAPs including tau and regulate MT dynamics [25, 26].

It is well documented that the composition of β -tubulin isotypes (i) affects MT dynamic instability [27, 28], (ii) their interaction with motor proteins [29], (iii) their binding to the anti-drugs [21, 22, 30] and (iv) different MAPs including tau [31, 32]. These tubulin isotypes show tissue specific expression as their relative proportion varies greatly in different type of cells [20, 33, 34]. It is also well established that binding of tau to the MT promote or demote microtubule polymerization [35]. However, the differential binding affinity of tau to the various β -tubulin isotypes

expressed in different types of cells is completely unknown. Therefore, we studied relative binding affinity of Tau repeat region R2 with neuronal specific β -tubulin isotypes namely β I, β IIb, and β III using molecular modeling [36].

2. Methodology

2.1 Sequence analysis and homology modeling of tubulin isotypes

In biological research, sequence analysis plays a major role as it has wide range of applications such as, (i) whole genome sequencing and annotation, (ii) identification of functional elements in the sequence, (iii) gene prediction, (iv) comparative genomics, (v) protein classification, (vi) protein and RNA structure prediction, (vii) evolutionary studies, etc. Protein sequences reveal the evolutionary history and hence, the events occurred during evolutions can be traced from the protein sequences.

The structure 6CVN.pdb is used as template structure for homology modeling of neuronal specific human tubulin isotypes namely β I, β IIb and β III tubulin (uniprot IDs Q9H4B7, Q9BVA1 and Q136509). The multiple sequence alignment of these sequence was performed using 'clustal omega' tool [37]. The multiple sequence alignment reveals that residue variations is mainly at the C-terminal tail when compared to the other regions of the protein. The high-resolution cryo-EM structure of $\beta/\alpha/\beta$ -tubulin bound with TauR2 was recently deposited in the RCSB structural databases [8] was used as a template to build β I/ α/β I-TauR2, β IIb/ α/β IIb-TauR2 and β III/ α/β III-TauR2 complexes. The structure for C-terminal tail was absent in the template structure (6CVN.pdb), therefore the tail region was modeled using the Modeler 9v20. Hereafter, template structure with modeled C-terminal tail region would be referred as 6CVN* in the further discussion.

Template based homology models for neuronal specific tubulin isotypes β I, β IIb, β III was build using Modeler 9v20 [38]. The least discrete optimized potential energy (DOPE) score model was selected for further use. The stereo-chemical properties of these modeled subunits were evaluated and validated using the GMQE score [39], verify3D [40], ERRAT score [41] and Ramachandran plot through PROCHECK [42]. The selected subunit models were further used to 6CVN*-TauR2, build β I/ α/β I-TauR2, β IIb/ α/β IIb-TauR2 and β III/ α/β III-TauR2. These complexes namely 6CVN-TauR2, 6CVN*-TauR2, β I/ α/β I-TauR2, β IIb/ α/β IIb-TauR2 and β III/ α/β III-TauR2 were further subjected for energy minimization to get their least energy state. Here we used Steepest Descent and Conjugate Gradient methods in Gromacs 2018.1 software for minimization [43]. The process of energy minimization is a numerical procedure aimed to find a minimum on the potential energy surface (PES) of the newly modeled conformation which mostly exists at a higher energy level. These minimized models were used as a starting input structures for molecular dynamics simulations to understand the binding mode and binding affinity of TauR2 towards neuronal specific tubulin isotypes β I, β II and β III.

2.2 Molecular dynamics simulations of tubulin-TauR2 complexes

Molecular dynamics (MD) simulation plays a key role in exploring the structure and function of biological macromolecules [44]. In MD simulations, the dynamic behavior of the molecule is studied as a function of time. Molecular dynamics is being routinely used to address various biological problems such as biomolecular interactions (Protein-protein, protein-DNA/RNA), molecular pathways, Drug-receptor interactions, dynamics of protein folding, protein aggregations, protein

structure prediction, etc. Tremendous development in high performance computing and simplicity of the basic MD algorithm has shortened the time required to perform molecular dynamics simulation and hence, studying larger systems became an easier task [45].

All atom molecular dynamics (MD) simulation was performed in explicit solvent on the modeled tubulin-TauR2 complexes (i.e. 6CVN-TauR2, 6CVN*-tau, β I/ α / β I-TauR2, β IIb/ α / β IIb-TauR2 and β III/ α / β III-TauR2) using GROMACS 2018.1 [43, 46]. The ‘Amber99SB-ILDN’ force field [47] was chosen for the MD simulation because it is well customized to handle the parameters for GTP, GDP and MG atoms which are the functional players of all the modeled tubulin-TauR2 complexes. The force field parameters for the GDP and GTP molecules were retrieved from the amber parameter database [48, 49]. The ‘xleap’ module of AmberTools was used to generate topology files and initial starting coordinates for all the complexes [50]. All the modeled tau-tubulin complexes were placed at the centre of a cubic shaped solvation box having dimension of 15 Å from the extent of the molecule and TIP3P water model was used for solvation. All the systems were neutralized by adding appropriate number of required counterions. The topology files generated using xleap module of AmberTools were converted to Gromacs compatible topologies with ParmEd tool [51]. Energy minimization was carried out in two steps, In the first step, steepest descent algorithm was used for 50,000 followed by the conjugate gradient [46]. The energy minimized models were equilibrated using canonical ensemble (NVT) followed by isothermal-isobaric ensemble (NPT) for 1 ns. In the NVT equilibration systems were heated to 300 K using V-rescale, a modified Berendsen thermostat [46]. These heated systems were further equilibrated using the Parrinello-Rahman barostat to maintain constant pressure of 1 bar. The production MD simulations were performed for 100 ns without restraining any atoms over all the tubulin-TauR2 complexes using parameters discussed in earlier study [52]. The PME method was used to treat long range electrostatic interactions [53, 54] and covalent bonds involving H-atoms were constrained by using ‘LINCS’ algorithm [55]. The 2 fs time step was set for integrating the newtonian equation during the MD simulation. Similar protocol was adopted to perform MD simulation on three additional systems (i) 6CVN* (without tau), (ii) free tau and (iii) 6CVN*-polyA (as negative control) having 27 amino acids residues. All the MD simulation trajectories were further analyzed by using the GROMACS 2018.1 inbuilt tools [43, 46]. The general parameters explaining the conformational stability such as Root Mean Square Deviation (RMSD), Root Mean Square Fluctuations (RMSF) and Radius of Gyration (Rg) were measured, and the equations used for calculation of these parameters are tabulated in the **Table 1**.

The primary sequence of a protein is a linear chain of amino acids linked by peptide bonds. There is a direct link between the protein sequence, structure and function. The secondary structure of a protein is comprised of coils, α -helices, β -sheets,

S. no.	Parameter	Equation	Component
1	RMSD	$RMSD = \sqrt{\frac{\sum_{i=1}^N d_i^2}{N}}$	d_i is the distance, ‘N’ is number of atoms
2	RMSF	$RMSF = \sqrt{\frac{\sum_{j=1}^t (x_i(t_j) - \bar{x}_i)^2}{t}}$	x_i is atom position at time t , reference position is \bar{x}_i
3	R _g	$R_g = \sqrt{\frac{\sum_{i=1}^N (x_i - x_{com})^2}{N}}$	x_{com} centre of mass, x_i is the distance at time t from their centre of mass

Table 1.
 Equations used to calculate RMSD, RMSF and R_g

β -bridge, bend, turn, coils, π -helix and 3_{10} -helices. DSSP is an algorithm developed by Kabsch and Sander to extract the secondary structural features based on atomic coordinates [56]. The overall stability of the structure is highly determined by the stable dynamics of these secondary structures and any significant changes in secondary structure attributes to the structural flexibility/fold as well as functional diversity of the protein. Hence, conformational changes in the secondary structure during MD simulation were analyzed using the DSSP programme [56]. The simulation movies over the entire trajectories were generated using the VMD software [57] and publication quality images were generated using the Biovia Discovery studio visualizer [58] and Chimera software [59].

2.3 Calculations of contact surface area (CSA) for tubulin-TauR2 complexes

Solvent Accessible Surface Area (SASA) is used to represent the degree of hydration of a biomolecule. SASA also be especially useful to quantify the stability of the biomolecular complexes in the aqueous medium. The C-terminal tail of the tubulin subunits is highly dynamic in nature and has no definite secondary structure, hence it affects the overall hydrophobic SASA. Therefore, interface of the MT (in this case tubulin trimer made up of $\beta/\alpha/\beta$ subunits) where TauR2 binds at the exterior surface has been selected for the calculating the precise CSA. The in-built gromacs tool “*gmx sasa*” [60] was used to calculate the SASA. In addition, SASA is also calculated for the tubulin subunits and the TauR2.

2.4 Binding affinity of tauR2 towards different neuronal specific tubulin isotypes

The biomolecular recognition pattern mainly depends on the binding ability of the interacting biomolecules. The binding affinity as well as the energy between the two interacting molecules can be calculated using various theoretical approaches like (i) Pathway methods such as Thermodynamic integration (TI) as well as Free energy perturbation (FEP) and (ii) End point methods such as Molecular Mechanics Poission-Boltzman Surface Area (MM/PBSA) and Molecular Mechanics Generalized Born Surface Area (MM/GBSA) [61]. In the present study, MM/PBSA approach was used to calculate relative binding energies of the simulated molecules. This MMPBSA approach is very popular, computationally less expensive, and has better accuracy even for the larger systems [62].

Here, the binding affinity between different neuronal specific tubulin isotypes and TauR2 was estimated by performing relative binding energy calculation similar to earlier studies [63–65]. The stable trajectory observed in between 70 ns to 100 ns was chosen to perform the binding energy calculations for all the tubulin-TauR2 complexes. The ‘*g_mmpbsa*’ tool v1.6 was used to perform binding energy calculation using MM/PBSA approach [66]. The parameters for the binding energy calculations were chosen from the earlier similar studies [52, 65, 67–69]. In the MMPBSA methods binding energy (ΔG_{bind}) of tubulin and TauR2 was calculated by using the following Eq. (1),

$$\Delta G_{\text{bind}} = \Delta G_{\text{tubulin-TauR2}} - (\Delta G_{\text{tubulin}} + \Delta G_{\text{TauR2}}) \quad (1)$$

Where, the $\Delta G_{\text{tubulin-TauR2}}$, $\Delta G_{\text{tubulin}}$ and ΔG_{TauR2} represents the average free energies of the complex (tubulin-TauR2), receptor (tubulin) and ligand (TauR2), respectively. The calculation of the entropic contribution in binding energy is

computationally expensive for a larger biomolecular complexes and hence it is omitted as similar to previous studies [21, 22, 70–72].

3. Results and discussion

In this chapter we employ sequence analysis, homology modeling, MD simulations, and binding energy calculation to (i) gain structural insights to the detailed binding mode, (ii) study atomic level tubulin isotypes-tauR2 interactions and (iii) study relative binding affinity between neuronal specific tubulin isotypes and TauR2.

3.1 Sequence analysis and homology modeling of neuronal specific tubulin isotypes

The residue composition of different β -tubulin isotypes mostly varies at the carboxy-terminal tail region as revealed by the multiple sequence alignment (**Figure 2**). The β I and β III tubulin isotypes have longer C-terminal tail regions when compared with the β IIb tubulin isotype. The β -tubulin sequence in the template structure i.e., 6CVN (chain A) and human β IIb tubulin isotypes show 98.65% sequence identity. These sequence variations in the tubulin isotypes are reported to regulate number of protofilaments in the MT and their stability [73]. These β -tubulin isotypes sequences were used to generate three-dimensional homology models using 6CVN as the template. The structures of β I, β IIb, β III tubulin isotypes were modeled using Modeler 9v20 [38]. The best homology model generated is selected using DOPE score. The DOPE score value for A and C chain of (i) β I subunits are -54299.89 and -54291.24 (ii) β IIb subunits are -53487.13 and -53054.42 and (iii) β III subunits are -53725.86 and -53054.42 . The quality of these models is accessed using GMQE score [74], Verify3D [40], Errat score [41], Z-score [75] and Ramachandran plot [76, 77]. The parameters describing the overall quality of the modeled neuronal specific β -tubulin subunits are shown in **Table 2**. The GMQE score provides an estimate of the accuracy of the modeled tertiary structure of neuronal specific β -tubulins. Here, GMQE score for all the modeled β -subunits is 0.98, which represents the accuracy of the generated model. Further, verify3D and ERRAT score also validates the quality of the generated models (**Table 1**). Ramachandran plots for all the modeled β -tubulin isotypes represents more than 98% of the residues occupy a favored region. The occupancy of amino acid residues in the Ramachandran plot is given in **Table 3**. These modeled structures of neuronal specific β -tubulin isotypes were used further to build the tubulin and TauR2 complexes such as β I/ α / β I-TauR2, β IIb/ α / β IIb-TauR2 and β III/ α / β III-TauR2 using 6CVN.pdb as a template structure. These modeled complexes were used as starting structures to perform MD simulations.

3.2 Structural stability of the tubulin-TauR2 complexes

The all atom MD simulations were performed on tubulin-TauR2 complexes namely 6CVN-TauR2, 6CVN*-TauR2, β I/ α / β I-TauR2, β IIb/ α / β IIb-TauR2, β III/ α / β III-TauR2 using Gromacs 2018.1 [78]. The stability of these tubulin-TauR2 complexes is accessed by plotting the potential energy during the simulation period, which highlight that all the complexes are well minimized, and simulation trajectories are well converged during the simulation period of 100 ns (**Figure 3**).

The parameters describing the stability of tau-tubulin complex such as RMSD (root mean square deviation), RMSF (root mean square fluctuation), and Rg (radius of gyration) was studied. The RMSD values for simulated tubulin-TauR2 complexes, tauR2 and backbone atoms of tubulin trimer without considering

Region	$\beta 1$ tubulin		$\beta 2$ tubulin		$\beta 3$ tubulin	
	Chain A	Chain C	Chain A	Chain C	Chain A	Chain C
% of most favored regions	98.4 (442)	98.9 (444)	98.9 (443)	98.9 (438)	98.9 (443)	98.9 (443)
% of additional allowed regions	1.3 (6)	0.9 (4)	0.7 (3)	1.1 (5)	1.1 (5)	0.7 (3)
% of outlier	0.2 (1)	0.2 (1)	0.4 (2)	0 (0)	0 (0)	0.4 (2)

Table 3.
 Ramachandran plot showing the percentage of residues in the different regions for tubulin isoforms obtained from the Ramachandran plot using PROCHECK.

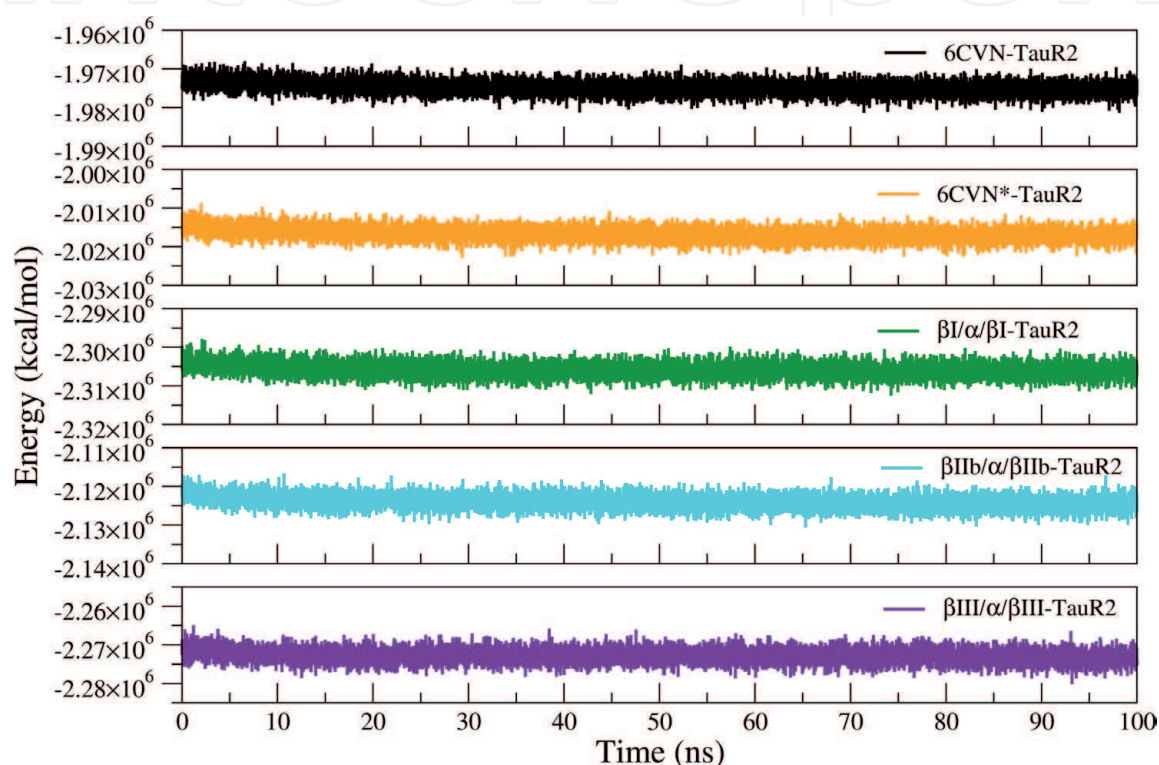


Figure 3.
 Energy Minimization Plot Potential energy over the simulation time plotted for 6CVN-TauR2 (black), 6CVN*-TauR2 (orange), $\beta I/\alpha/\beta I$ -TauR2 (green), $\beta IIb/\alpha/\beta IIb$ -TauR2 (cyan), $\beta III/\alpha/\beta III$ -TauR2 (violet) are shown.

of TauR2 bound to $\beta III/\alpha/\beta III$ tubulin trimer expresses stable dynamics during the simulation. The complex 6CVN-TauR2 is stabilized at higher RMSD values, the primary reason for this elevated RMSD value is absence of C-tail region which highlights the importance of C-terminal tail in the stabilizing tubulin-TauR2 complex. Average backbone RMSD value is converged at ~ 3.5 Å hence represents the equilibration of all above simulated systems (**Figure 5**). The molecular dynamics simulation movies reveals the stable dynamics of all the simulated systems 6CVN-TauR2, 6CVN*-TauR2, $\beta I/\alpha/\beta I$ -TauR2, $\beta IIb/\alpha/\beta IIb$ -TauR2 and $\beta III/\alpha/\beta III$ -TauR2 (<https://youtu.be/mU2Jrm5jusY>, <https://youtu.be/Sr2JiQWha9A>, <https://youtu.be/U5S6X-o8kO8>, <https://youtu.be/xYbm9eCsE4Q>, <https://youtu.be/0H0CsmveT24>) respectively. Further, specificity of TauR2 towards tubulin subunits was accessed by replacing the TauR2 with negative control 'polyA' peptide of same length. Interestingly, This system having negative control poly A bound to 6CVN* shows the weak binding during the simulation. These weaker interactions of polyA peptide with tubulin subunits (<https://youtu.be/ZEFQblQTHqk>) represents that tauR2 has specificity towards tubulin subunits. s.

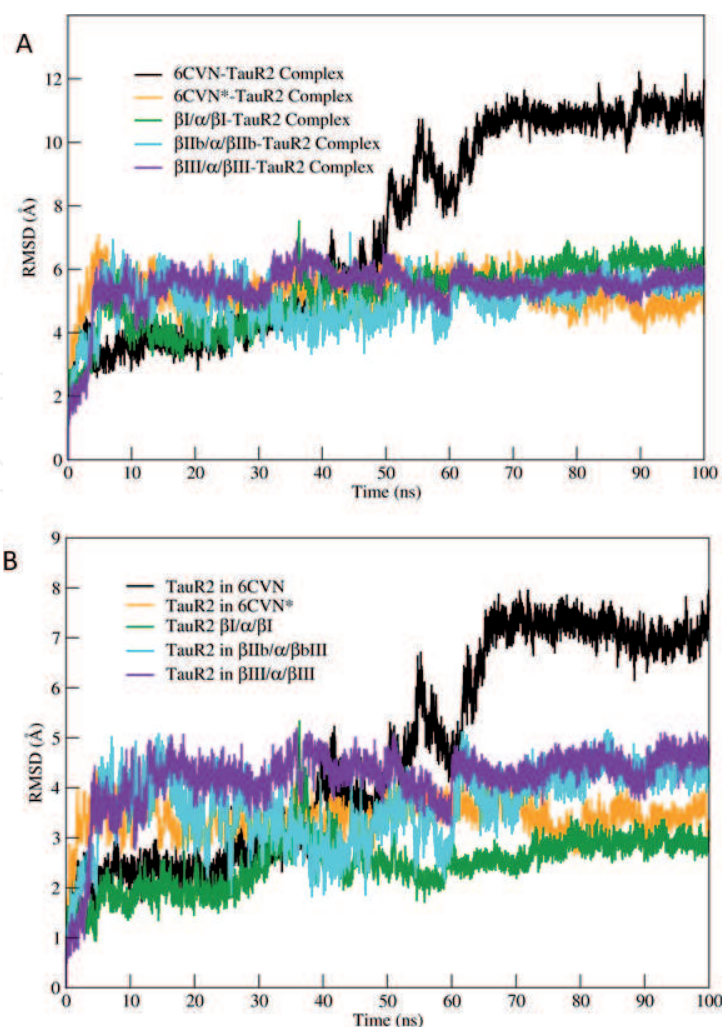


Figure 4. Stability of the tubulin-TauR2 complex and TauR2. (A) The Root mean square deviation values (RMSD) for tubulin-tauR2 complexes. RMSD values for 6CVN, 6CVN*, $\beta I/\alpha/\beta I$, $\beta IIb/\alpha/\beta IIb$ and $\beta III/\alpha/\beta III$ have been plotted in black, orange, green, cyan and violet, respectively. (B) The Root mean square deviation values for TauR2 shown using same color Scheme as in (A).

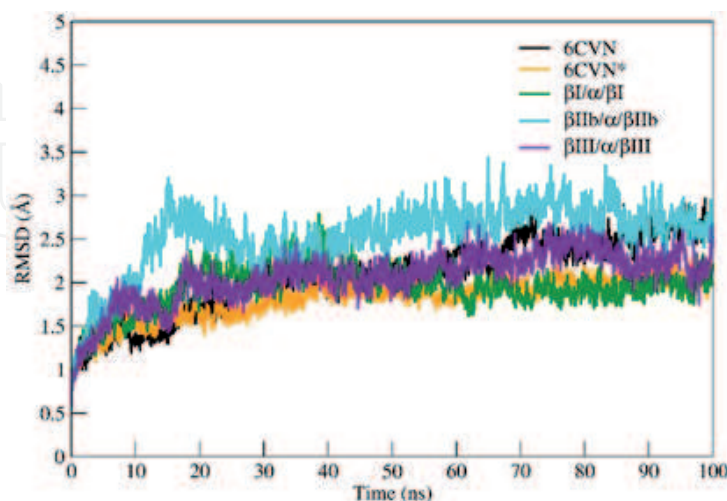


Figure 5. Backbone Root mean square deviation for different tubulin subunits. Color scheme is same as Figure 3.

3.3 Residue fluctuations of tubulin subunits and TauR2

The flexibility of tubulin trimers systems and TauR2 has been studied using RMSF analysis. For this analysis $C\alpha$ -atom from the backbone was selected to get fluctuations in the overall protein. **Figure 6** represents the RMSF for tubulin

subunits and TauR2. The residues from the H12 helix of β -tubulin and the C-terminal tail region (residue 400–451) show significant decrease in the RMSF

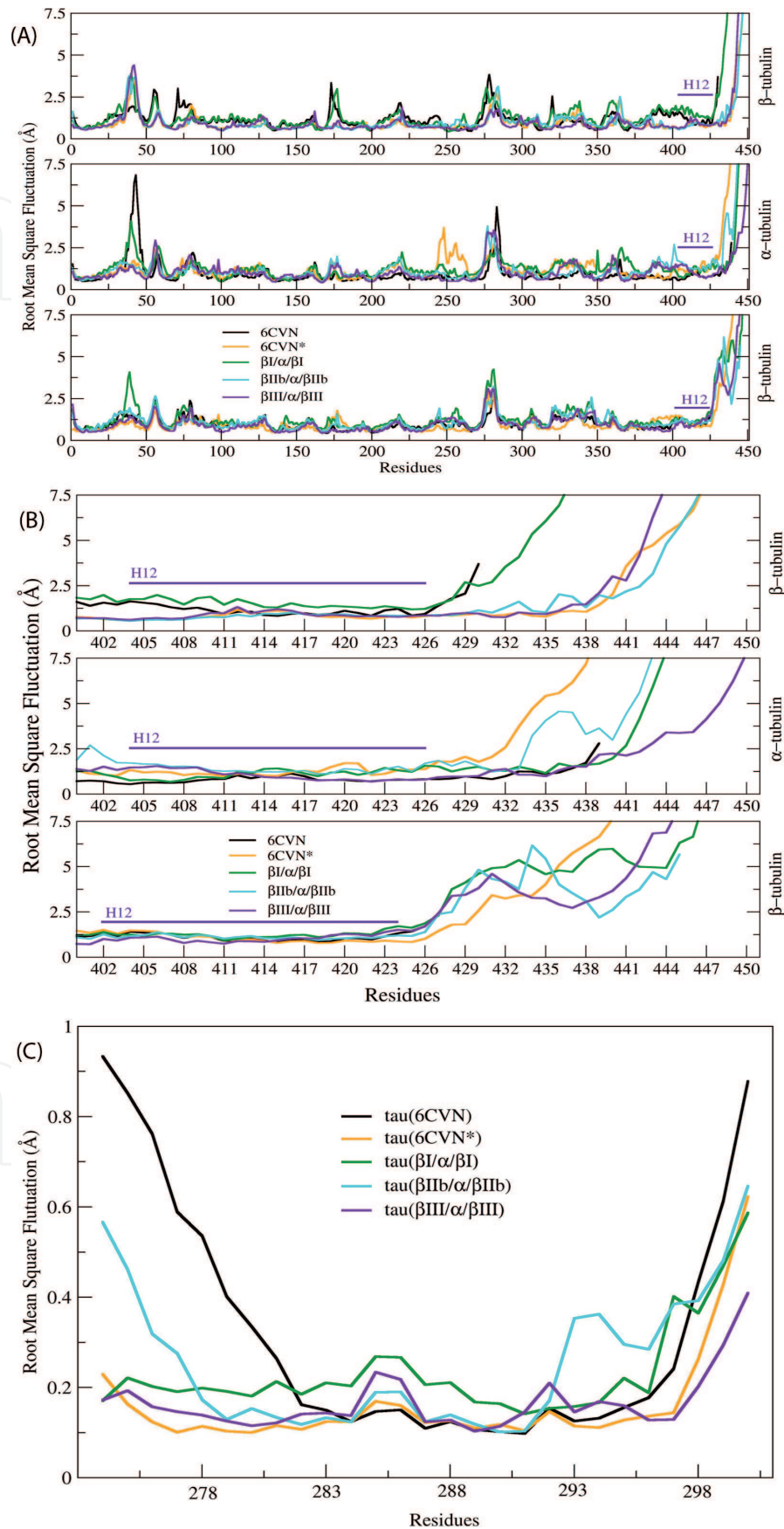


Figure 6. Root mean square fluctuations (RMSF) of different β / α β tubulin subunits and TauR2 (A) RMSF of different β / α β tubulin subunits (B) Magnified view of their C-terminal H12 helix and tail regions (C) RMSF of TauR2 bound with different β / α β tubulin subunits observed during the simulations⁵. Color scheme is same as Figure 3.

values, as their free dynamics is arrested by tau binding (**Figure 6A and B**). RMSF values for the tubulin β -subunits in the systems 6CVN*, β I**II**/ α / β I**II** and β I**III**/ α / β I**III** are lesser than those of 6CVN and β I/ α / β I tubulin subunits (**Figure 6B**). This observation also highlights the binding of TauR2 at the interdimer interface where residual fluctuations are less. However, the part of C-tail region which has no direct contact with TauR2 is highly flexible (**Figure 6B**). The H12 helix and C-terminal tail region of the tubulin subunits significantly contribute to the non-covalent interactions resulting towards stronger binding of TauR2. Therefore, these intermolecular interactions were analyzed in detail and are discussed in the section '*Intermolecular interactions between tubulin and tau*'. Further, atomic $C\alpha$ -fluctuations of TauR2 (**Figure 6C**) was also studied for better understanding its conformational behavior during the MD simulations. It is surprising to observe highest fluctuations at the N- and C-terminal region in TauR2 bound to 6CVN, where the C-terminal tail region is absent (**Figure 6C**). Interestingly, residual fluctuations expressed by TauR2 bound to β I**III**/ α / β I**III**-tau complex are much lesser as compared to 6CVN*-TauR2, β I/ α / β I-TauR2 and β I**II**/ α / β I**II**-TauR2 complexes (**Figure 6C**). This also proves that the C-terminal tail region of tubulin subunits plays an important role in the binding of TauR2.

Overall, RMSF analysis suggests the significance of H12-helix and C-terminal tail region in stabilization of the microtubule by binding of tau repeats (TauR2) and it also reveals the greater affinity of TauR2 towards β I**III** tubulin isotypes which are overexpressed in neuronal cells and brain. Further compactness of all the tubulin-TauR2 complexes was explored by calculating the radius of gyration (R_g) and this analysis is discussed in the next section.

3.4 Compactness of tubulin-TauR2 complexes

The radius of gyration (R_g) indicates the level of compactness of the protein system which is helpful in getting an insight into the stability of the protein-protein complex. It also helps to understand folding or unfolding of protein structure during the simulation. The R_g values for all the studied tubulin-TauR2 complex ranges from 38.8–40.5 Å (**Figure 7A**). The complex β I**III**/ α / β I**III**-TauR2 shows stable R_g value for the entire simulation period however other complexes 6CVN-TauR2 6CVN*-TauR2, β I/ α / β I-TauR2, β I**II**/ α / β I**II**-TauR2 show variations in their R_g values. The absence of C-terminal tail region in the complex 6CVN-TauR2 leads to the less R_g values when compared to other tubulin-TauR2 (**Figure 7A**). **Figure 7B** represents the R_g values of only TauR2 in different tubulin-TauR2 complexes. The R_g values for TauR2 shows fluctuations between 17.5 to 20 Å in case of 6CVN*, β I**II**/ α / β I**II**, and β I**III**/ α / β I**III** complexes except for β I/ α / β I complex (**Figure 7B**). The β I**III** tubulin subunits show R_g value of ~18 Å and β I tubulin subunits have largest R_g value of 22.5 Å as shown in **Figure 7B**. On the other hand, TauR2 bound to 6CVN shows uninterrupted decline in R_g values from 21.5 Å to 16.5 Å. This analysis also highlights the importance of C-terminal tail region in the stable binding of tau (**Figure 7B**). It is important to note that β I**III** tubulin subunits (**Figure 8**) have R_g values like that of β I**III**/ α / β I**III**-TauR2 complex (**Figure 7A**). This highlights that the tubulin subunits composed of β I**III** tubulin isotype are structurally stable after binding to the TauR2. Thus, calculation of R_g values for tubulin-TauR2 complexes, tubulin subunits and TauR2 reveals (i) structural stability of the β I**III**/ α / β I**III**-tau complex over other complexes and (ii) importance of the C-terminal tail region in the binding of

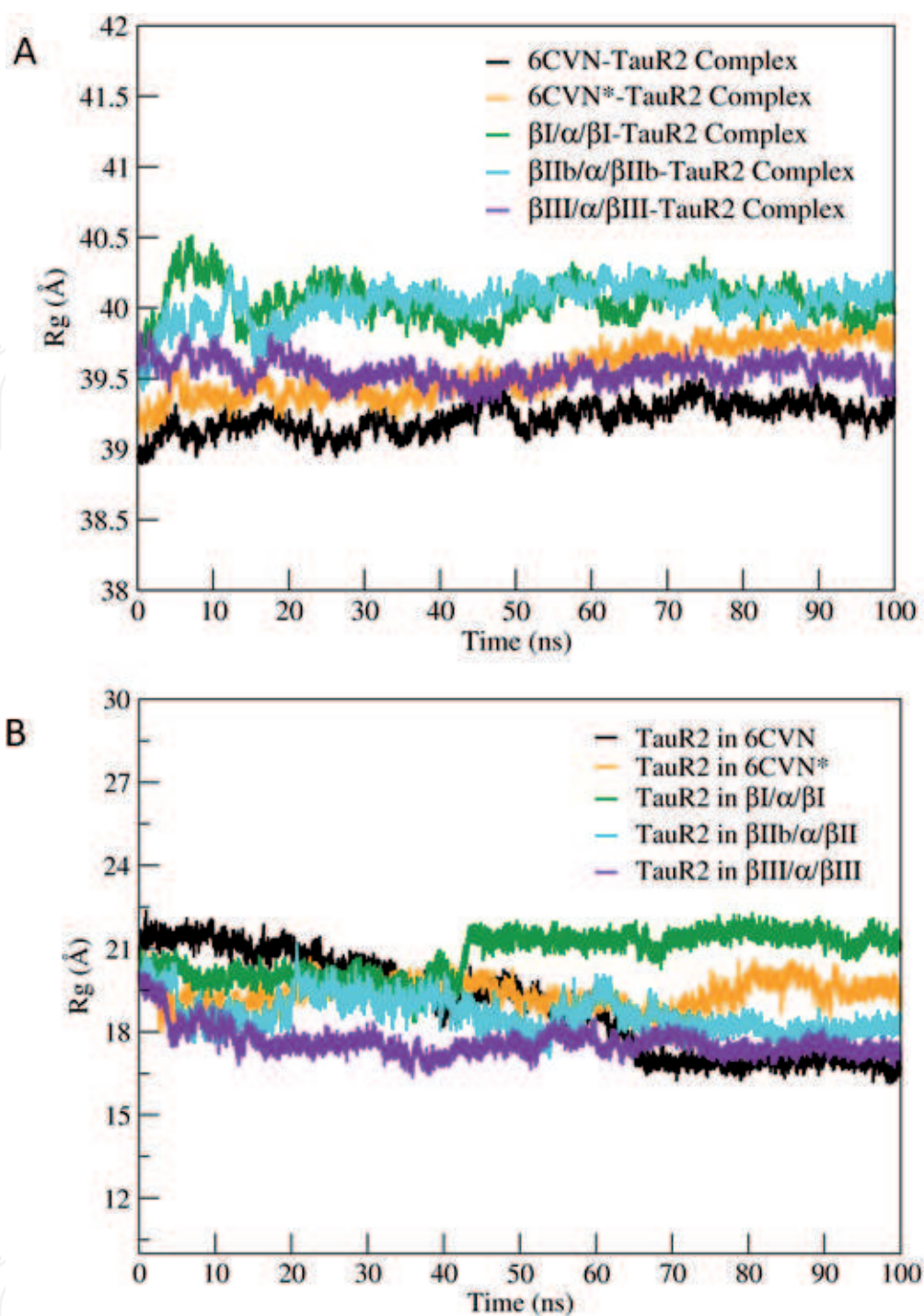


Figure 7. Radius of Gyration (R_g) of different tubulin-TauR2 complexes and TauR2. (A) R_g of 6CVN-TauR2 (black), 6CVN*-TauR2 (orange), β I/ α / β I-TauR2 (green), β IIb/ α / β IIb-TauR2 (cyan), β III/ α / β III-TauR2 (violet) (B) R_g for TauR2 in different tubulin-TauR2 complexes. Color scheme same as Figure 3.

TauR2. Contact surface area (CSA) and solvent accessible surface area (SASA) was calculated using 'gmx sasa' tool of gromacs to understand the exposure of the interface residues of tubulin subunits bound to the TauR2 [46].

3.5 Contact surface area (CSA) and solvent accessible surface area for tubulin-TauR2 complexes

The CSA and SASA describes the accessibility of a binding interface and protein surface to the solvent, respectively. It is well documented that, TauR2 binds

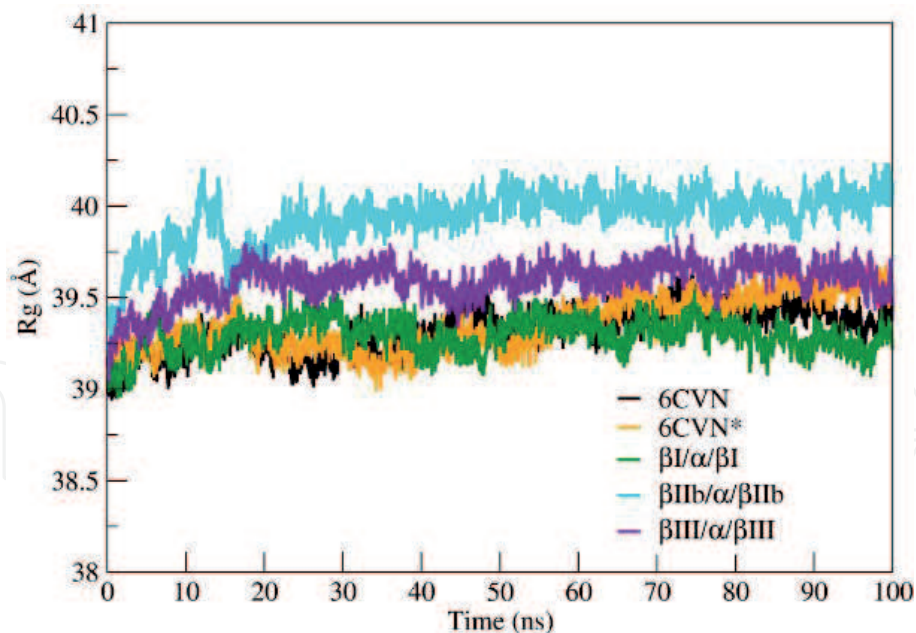


Figure 8.
Radius of Gyration for different tubulin isotypes. Color scheme is same as **Figure 3**.

to the MT exterior surface via C-terminal tail region [8, 79–82]. Therefore, initially contact surface area (CSA) of the interface between the TauR2 and tubulin trimer, was calculated, without considering flexible C-terminal tail region. The CSA of β III/ α / β III is very less when compared to other tubulin isotypes (**Figure 9A**) this represents the tight binding of TauR2 to the β III/ α / β III tubulin subunits. The higher CSA for β I/ α / β I-TauR2 complex indicates weaker binding of the TauR2 to the β I/ α / β I tubulin subunits. Furthermore, least SASA in complex β III/ α / β III-TauR2 represents tight binding of TauR2 to the β III/ α / β III (**Figure 9B**). On the other hand, higher hydrophobic SASA of the complex β I/ α / β I-TauR2 indicate the exposure of hydrophobic residues which are responsible for loss of native contacts between tubulin and TauR2. The SASA for 6CVN*, β I/ α / β I, β IIb/ α / β IIb, β III/ α / β III shows higher SASA values between 4900 and 5400 Å² when compared to 6CVN-TauR2 (~4500 Å²) due to the presence of C-terminal tail region (**Figure 10**). To get detailed understanding of the atomic-level interaction between tubulin isotypes and TauR2, further hydrogen bonding interactions were estimated during simulation and in the MD simulated end-structures obtained from trajectory.

3.6 Intermolecular interactions between tubulin and TauR2 in tubulin-TauR2 complexes

The total number of hydrogen bonds formed between tubulin isotypes and TauR2 during the MD simulations are calculated using in-built ‘*gmx hbond*’ command [46]. The cut-off value for the measurement of H-bond was set to 3.4 Å. Consistent H-bond formation was observed throughout the MD simulation in all tubulin-TauR2 complexes. The average number of H-bonds roughly varies between 10 to 20 as shown in **Figure 11**. The details of atom participating in the hydrogen bonding interactions present between tubulin isotypes and TauR2 in the MD simulation end-structures are listed in **Table 4**. All the hydrophobic interactions participating in the formation of stable tubulin-TauR2 complexes are listed in **Table 5**. The β III/ α / β III-TauR2 complex shows the maximum number of electrostatic interactions when compared to other

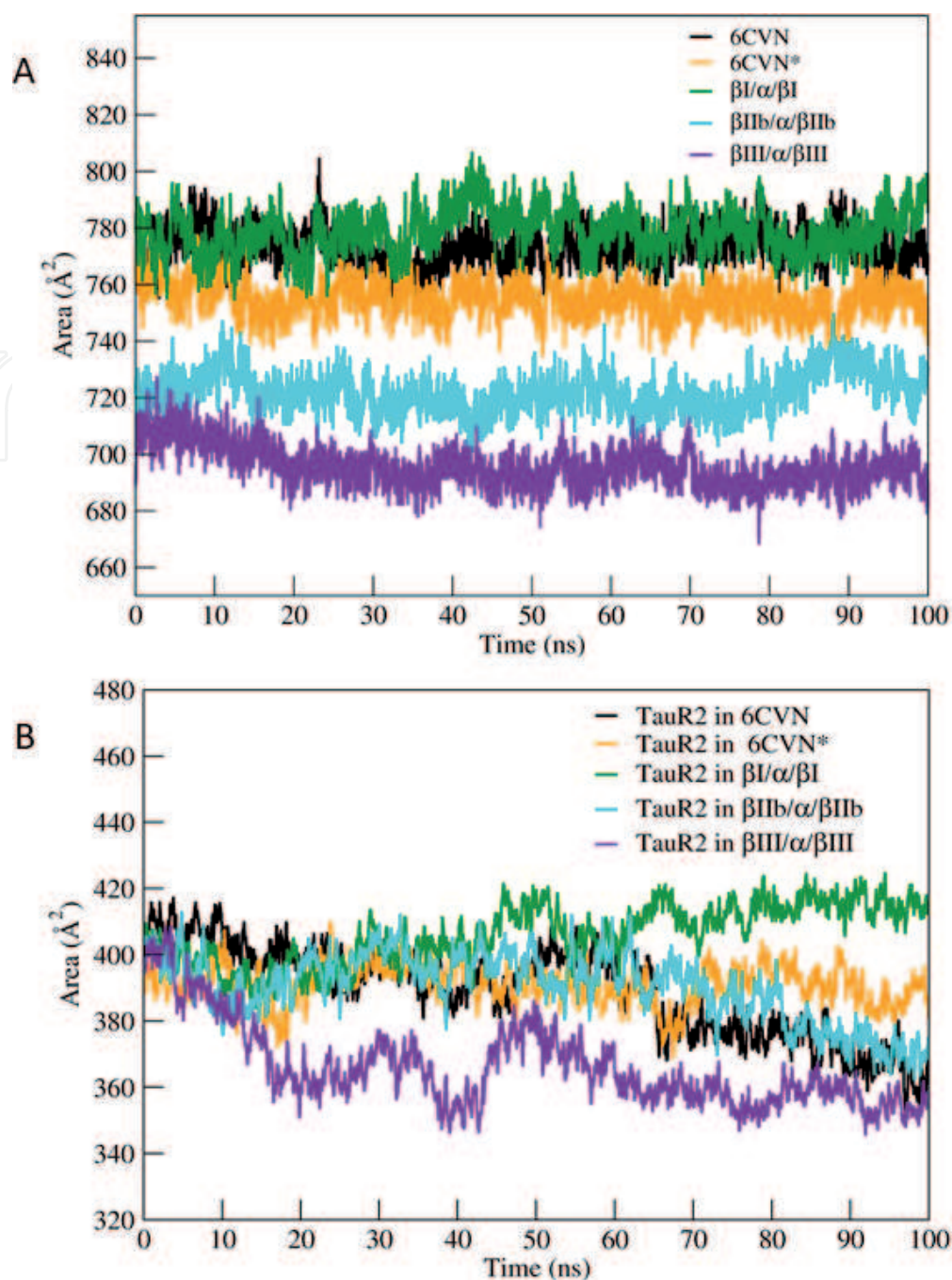


Figure 9. Contact surface area (CSA) and solvent accessible surface area (SASA) of different β/α -tubulin subunits and TauR2. (A) CSA for different 6CVN-TauR2 (black), 6CVN*-TauR2 (orange), β I/ α β I-TauR2 (green), β IIb/ α / β IIb-TauR2 (cyan), β III/ α / β III-TauR2 (violet) complexes. (B) hydrophobic SASA for tubulin isotype bound TauR2. Color scheme same as Figure 3.

tubulin-TauR2 complexes (Table 6). Further, to understand the role of TauR2 in stabilizing tubulin subunits, secondary structure analysis on TauR2 was done using DSSP.

3.7 Conformational changes in TauR2 upon tubulin binding

Tau belongs to the class of intrinsically disordered proteins for which no definitive secondary structure exists. Hence their structure determination is difficult by using existing biophysical techniques like X-ray crystallography and NMR. Previous experimental observations propose that tau repeat undergoes a conformational changes from the disordered to ordered state when it binds to the MT [2, 83–86].

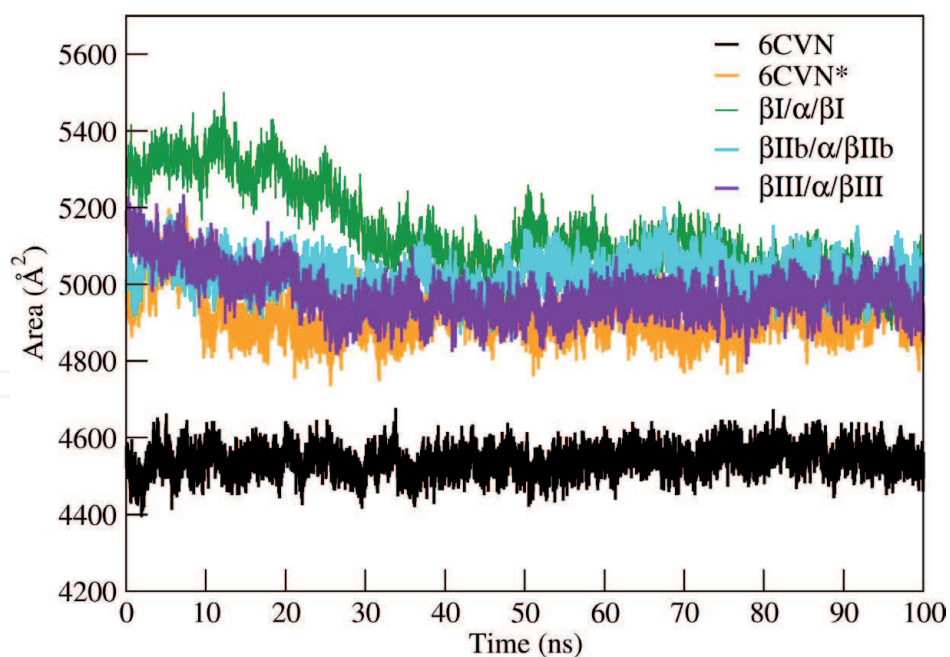


Figure 10.

Solvent accessible surface area for different tubulin subunits. SASA plotted for 6CVN (black), 6CVN* (orange), $\beta I/\alpha/\beta I$ (green), $\beta IIb/\alpha/\beta IIb$ (cyan), $\beta III/\alpha/\beta III$ (violet) are shown.

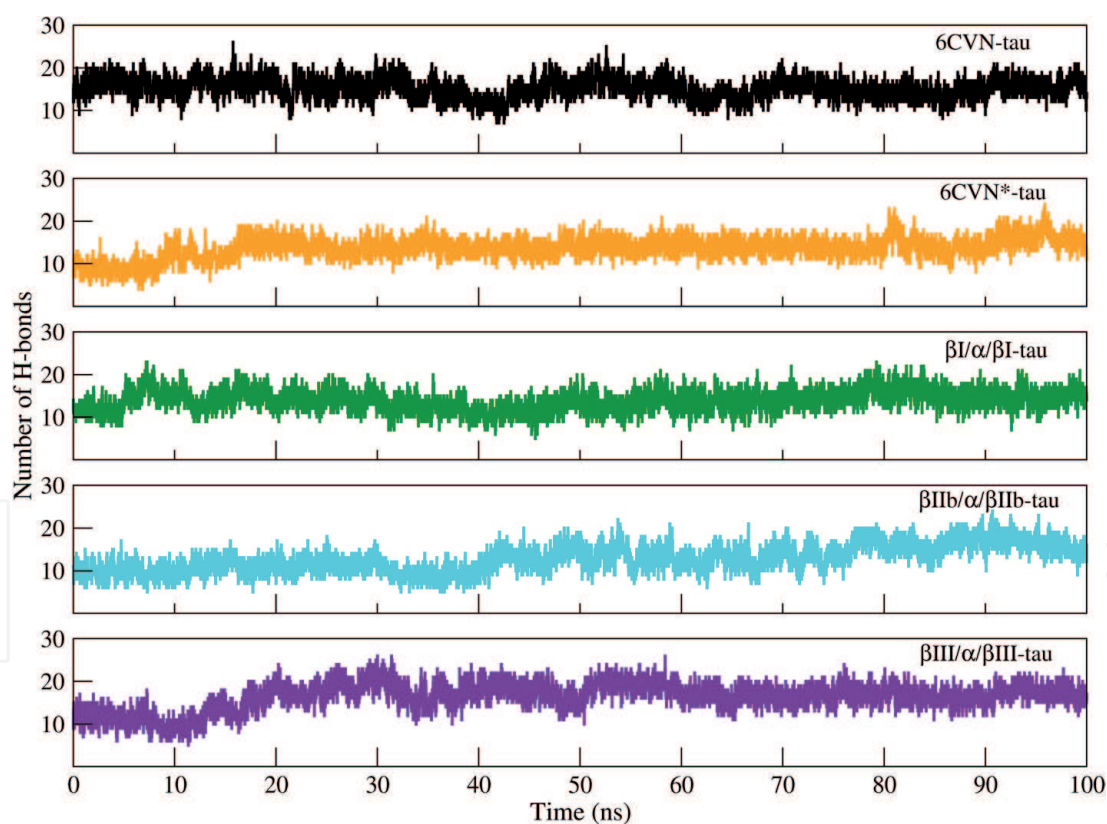


Figure 11.

The number of hydrogen bonds formed in between tubulin subunits and TauR2 during MD simulation. Color scheme is same as Figure 3.

Hence, the secondary structural changes during the MD simulations in the TauR2 were studied using DSSP [56]. **Figure 12** represents conformational changes in the secondary structure of TauR2 upon binding to the tubulin. TauR2 in 6CVN- TauR2 (**Figure 12A**) and 6CVN*- TauR2 complexes (**Figure 12B**) show formation of short and transient 3_{10} -helix during the simulation. The TauR2 in $\beta I/\alpha/\beta I$ - TauR2 complex does not form either α -helix or transient 3_{10} -helix as shown in **Figure 12C**. The

System	Atoms involved in H-bonding	Distance (Å)	Angle (°)
6CVN-TauR2	D: SER16: HG - B: GLU434:OE2	1.55968	170.912
	C: LYS392:HZ2 - D: ASP22:OD1	1.79981	155.003
	D: SER20:H - B: GLU434:OE1	1.80025	149.621
	D: CYS18:H - B: ASP431:OD1	1.8071	147.422
	D: GLY19:H - B: ASP431:OD1	1.81516	170.051
	D: ASN23:HD21 - C: PHE389:O	1.83614	168.422
	D: ILE5:H - B: GLU415:OE1	1.87843	148.138
	B: ARG402:HH22 - D: LYS7:O	1.95256	131.998
	D: LYS21:HZ3 - B: ASP438:O	1.96835	128.744
	C: ARG391: HE - D: SER20:O	1.97398	162.451
	D: ASN6:H - B: GLU415:OE2	1.97803	165.667
	D: LYS17:HZ2 - B: ASP424:OD1	2.01656	167.691
	6CVN ⁺ -TauR2	A: SER16: HG - E: ASP431:OD2	1.56368
A: ASN6:HD21 - G: GLN433:OE1		1.68122	165.335
A: LYS1:HZ1 - G: ASP417:OD1		1.73491	152.719
A: LYS7:HN - E: ALA400:O		1.75148	168.412
A: SER12: HG - A: ASP10:OD2		1.77457	163.204
E: LYS401:HZ1 - A: ASN6:OD1		1.77792	156.289
A: SER20:HN - E: GLU434:O		1.8254	168.05
A: ILE4:HN - G: GLN424:OE1		1.85744	159.004
F: ARG391:HH21 - A: SER20: OG		1.88141	150.648
A: LYS17:HN - E: ASP431:OD2		1.88237	156.579
A: LYS1:HT2 - G: ASP417:OD2		1.93321	163.221
A: LYS25:HZ2 - A: VAL27: OXT		1.95566	155.991
F: ARG391: HE - A: SER20:O		1.95954	137.171
A: SER12:HN - A: ASP10:OD2		1.97395	166.966
A: VAL2:HN - G: GLU421:OE2		1.97952	167.491
A: SER20: HG - E: TYR262: OH		2.01579	158.876
A: CYS18:HN - E: ASP431:OD2		2.04985	143.832
A: ASP22:HN - A: ASP22:OD1		2.06458	123.428
βI/α/βI-TauR2	D: SER20: HG - B: GLU434:OE2	1.71015	154.981
	D: LYS17:H - B: ASP431:OD2	1.73879	154.124
	D: SER16: HG - B: ASP431:OD2	1.75545	159.778
	D: VAL2:H - A: GLU421:OE1	1.79605	175.632
	D: SER20:H - B: GLU434:OE2	1.79906	165.806
	D: LYS21:HZ1 - B: GLU434:O	1.82861	143.493
	B: LYS430:HZ2 - D: VAL14:O	1.84508	147.656
	D: ASN23:HD22 - C: PHE389:O	1.87483	147.025
	D: LYS1:H3 - A: ASP417:OD1	1.96013	159.665
	D: LYS7:H - B: ALA400:O	2.03926	154.297
	D: ILE4:H - A: GLN424:OE1	2.05966	141.181

System	Atoms involved in H-bonding	Distance (Å)	Angle (°)
β IIb/ α / β IIb-TauR2	A: SER16: HG - E: ASP431:OD1	1.71023	174.429
	A: LYS17:HZ2 - E: ASP424:OD2	1.72125	162.879
	A: LYS1:HT2 - F: GLU421:OE2	1.73767	160.093
	A: LYS25:HZ2 - E: GLU445:OE1	1.7524	156.386
	A: LYS7:HN - E: ALA400:O	1.7726	158.577
	A: ASN6:HD22 - F: ASP431:OD1	1.88399	166.501
	A: LYS17:HN - E: ASP431:OD1	1.90489	145.148
	E: ARG402:HH12 - A: LYS7:O	1.90591	147.259
	A: VAL27:HN - E: GLU445:OE1	1.92907	160.86
	A: CYS18:HN - E: ASP431:OD1	2.03765	145.506
	A: LYS25:HZ3 - E: GLU446:O	2.04646	165.654
	F: GLN424:HE21 - A: LYS1:O	2.06218	173.384
	β III/ α / β III-TauR2	A: SER16: HG - E: ASP431:OD1	1.57372
A: LYS21:HZ1 - E: GLU443:OE2		1.74362	173.969
F: GLN424:HE21 - A: VAL2:O		1.79549	177.625
A: GLN15:HE21 - E: GLU443:OE2		1.81621	154.684
A: LYS8:HZ3 - F: GLU433:OE1		1.84962	164.797
A: LYS8:HZ1 - E: ASP396:OD1		1.85984	168.252
G: ARG391:HH11 - A: ASN23:OD1		1.89423	162.494
E: GLY442:HN - A: ILE24:O		1.93324	171.538
A: LYS17:HN - E: ASP431:OD1		1.99492	142.974
A: CYS18: HG - E: ASP431:OD1		2.0734	155.708

Table 4.
Hydrogen bonding interaction between tubulin subunits and TauR2 after molecular dynamics simulations.

System	Hydrophobic Interactions	Distance (Å)
6CVN-TauR2	B: ALA427 - D: LYS17	4.23972
	B: ARG264 - D: CYS18	4.32305
	B: ALA426 - D: VAL14	4.34456
	B: ARG402 - D: ILE4	5.12692
	B: VAL409 - D: ILE4	5.16258
	B: ARG422 - D: LEU11	5.2126
	B: ALA427 - D: VAL14	5.2724
	6CVN ⁺ -TauR2	E: ALA426 - A: VAL14
E: ALA426 - A: LEU11		4.1983
E: ALA400 - A: LYS8		4.29681
G: PHE260 - A: ILE4		4.3943
A: VAL2 - G:PRO261		4.85577
A: LEU9 - A: LEU11		5.10635
A: LYS21 - E: VAL437		5.11425
E: ALA427 - A: VAL14		5.28218
A: VAL14 - A: LEU11		5.3507
E: ARG422 - A: LEU9		5.37331
A: VAL2 - A: ILE4	5.42169	

System	Hydrophobic Interactions	Distance (Å)
β I/ α / β I-TauR2	B: ALA426 - D: LEU11	4.086
	B: ALA426 - D: VAL14	4.25902
	A: PHE425 - D: ILE4	4.29071
	B: ALA427 - D: VAL14	4.57533
	A: PHE260 - D: VAL2	4.62894
	B: TYR262 - D: CYS18	4.75533
	B:PRO263 - D: LYS17	4.89022
	B: ARG402 - D: LYS7	4.99921
	D: CYS18 - B: VAL435	5.09522
	B: ARG422 - D: LEU9	5.15149
	B: LYS430 - D: VAL14	5.38523
	A: ALA428 - D: ILE4	5.40848
	B: VAL440 - D: LYS21	5.41789
	C: ILE405 - D: ILE24	5.46457
β IIb/ α / β IIb-TauR2	E: ALA427 - A: LYS17	3.91294
	E: ALA426 - A: VAL14	3.93471
	E: ALA426 - A: LEU11	4.19609
	A: CYS18 - E: ARG264	4.36259
	E: ALA400 - A: LYS8	4.4046
	A: CYS18 - E:PRO263	5.04073
	A: CYS18 - E: ILE265	5.21553
	G: LYS392 - A: ILE24	5.27213
	E: TYR399 - A: LEU9	5.32769
β III/ α / β III-TauR2	E: ALA426 - A: LEU11	3.83867
	E: ALA426 - A: VAL14	4.14469
	E: ALA427 - A: LYS17	4.22472
	E: ALA427 - A: VAL14	4.83218
	E: ARG422 - A: LEU11	4.84097
	A: LYS25 - E: VAL437	5.06163
	A: CYS18 - E: ARG264	5.14951
	E: ARG422 - A: LEU9	5.48905

Table 5.
 Hydrophobic interactions between different $\beta/\alpha/\beta$ -tubulin isoforms and TauR2 after molecular dynamics simulations.

TauR2 in β IIb/ α / β IIb-TauR2 complex shows the formation of short-lived α -helix and 3_{10} -helix (**Figure 12D**). The terminal residues of TauR2 from Ser293 to Val300 in β III/ α / β III-TauR2 complex () undergoes turn to α -helix conformational transition (**Figure 12E**). Therefore, it is proposed that this conformational transition of TauR2 from disordered to ordered state promotes the stable binding of TauR2 with the β III/ α / β III tubulin subunits.

Systems	Electrostatic interactions	Distance (Å)
6CVN-TauR2	D: LYS8:NZ - A: ALA430:O	4.04432
	D: LYS21:NZ - B: SER439:O	4.66847
	D: LYS25:NZ - B: GLU434:OE2	4.90999
	D: LYS21:NZ - B: GLU434:OE1	5.38615
6CVN [*] -TauR2	A: LYS1: N - G: GLU421:OE2	4.85022
	A: LYS7:NZ - E: GLU415:OE1	4.9846
	A: LYS25:NZ - E: GLU441:OE1	5.12197
	A: LYS17:NZ - E: ASP424:OD2	5.27557
β I/ α / β I-TauR2	D: LYS1: N - A: GLU421:OE1	2.86182
	D: LYS25:NZ - C: GLU412:OE1	4.31321
	D: LYS7:NZ - B: GLU415:OE1	4.45715
	D: LYS21:NZ - B: GLU434:OE2	4.75044
β I II / α / β I II -TauR2	A: LYS21:NZ - E: GLU434:OE2	4.3529
	A: LYS8:NZ - E: ASP396:OD2	5.021
β I III / α / β I III -TauR2	A: LYS25:NZ - E: GLU434:OE2	2.68494
	A: LYS25:NZ - E: GLU450:OE2	2.85019
	A: LYS1: N - F: ASP417:OD2	2.91844
	A: LYS1: N - F: GLU421:OE2	4.28381
	A: LYS7:NZ - E: GLU415:OE1	4.31182
	A: LYS21:NZ - E: GLU434:OE1	4.48844
	A: LYS17:NZ - E: ASP424:OD2	4.70401
	G: LYS392:NZ - A: ASP22:OD2	4.95323
A: LYS21:NZ - E: GLU450:OE2	5.37409	

Table 6.

Electrostatic interactions between different $\beta/\alpha/\beta$ -tubulin isotypes and TauR2 after molecular dynamics simulations.

3.8 Relative binding affinity of TauR2 towards neuronal specific tubulin isotypes

The relative binding affinity of TauR2 towards neuronal specific tubulin isotypes ($\beta/\alpha/\beta$) was analyzed by performing MMPBSA calculations for complexes 6CVN-tau, 6CVN^{*}-tau, β I/ α / β I-tau, β I**II**/ α / β I**II**-tau and β I**III**/ α / β I**III**-tau etc. The energy components that govern the binding energy are recorded in **Table 7**. This analysis reveals that, β I**III**/ α / β I**III**-tau complex shows most favorable interactions while 6CVN-tau complex is least favorable as supported by the binding energy values listed in **Table 7**. Thus, it is interesting to note the significance of C-terminal tail of the tubulin subunits in the stable binding of the tau repeat R2 to stabilize this complex. The order of calculated binding energy in between TauR2 with neuronal specific tubulin-TauR2 complexes is β I**III**/ α / β I**III** > β I**II**/ α / β I**II** > 6CVN^{*} > β I/ α / β I > 6CVN. The electrostatic interactions in these complexes contribute significantly to the binding energy particularly in β I**III**/ α / β I**III**-TauR2 and β I**II**/ α / β I**II**-TauR2 complexes when compared to the 6CVN and β I/ α / β I tubulin subunits (**Table 7**). The complex β I/ α / β I-TauR2 exhibits higher binding energy leading to its weaker affinity towards TauR2. In addition to β I**III**/ α / β I**III**-TauR2 the complex β I**II**/ α / β I**II**-TauR2 also

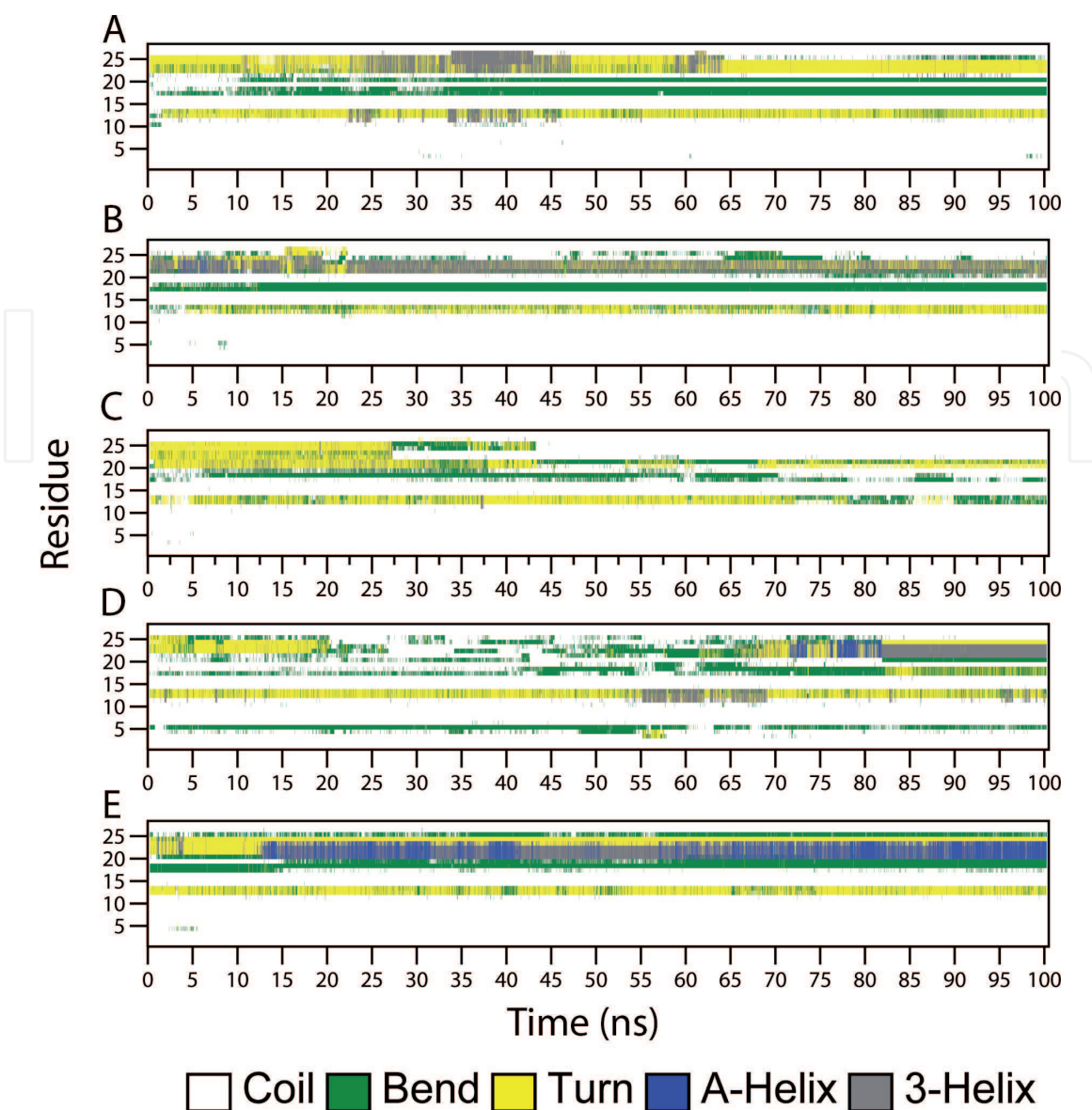


Figure 12. The secondary structure changes during MD simulation using DSSP for TauR2. Secondary structure changes observed in (A) 6CVN-TauR2 (B) 6CVN*-TauR2 (C) $\beta I/\alpha/\beta I$ -TauR2, (D) $\beta IIb/\alpha/\beta IIb$ -TauR2 and (E) $\beta III/\alpha/\beta III$ -TauR2.

System	6CVN	6CVN*	$\beta I/\alpha/\beta I$	$\beta II/\alpha/\beta II$	$\beta III/\alpha/\beta III$
Vdw	-97.25 ± 0.55	-131.17 ± 0.62	-133.38 ± 0.69	-124.36 ± 0.60	-125.24 ± 0.59
Elec	-1232.33 ± 3.43	-1534.36 ± 3.12	-1423.07 ± 2.77	-1659.30 ± 4.68	-1768.65 ± 2.77
Polar	413.98 ± 4.73	349.43 ± 4.18	439.27 ± 2.95	433.79 ± 4.13	505.14 ± 2.92
SASA	-12.35 ± 0.06	-15.12 ± 0.07	-17.05 ± 0.05	-15.66 ± 0.06	-16.04 ± 0.05
Binding Energy	-927.87 ± 3.15	-1331.15 ± 3.19	-1134.13 ± 1.13	-1365.226 ± 2.26	-1404.7 ± 1.84

Table 7. The relative binding energy of the tubulin-TauR2 complexes calculated using MMPBSA. All energies are given in kcal/Mol.

exhibits relatively higher affinity towards TauR2 compared to rest other complexes. Further, contribution of the individual residues in the binding energy has been investigated by calculating the decomposition energy for each residue. This analysis reveals that, residues from the H12 helix and C-terminal tail of tubulin subunits

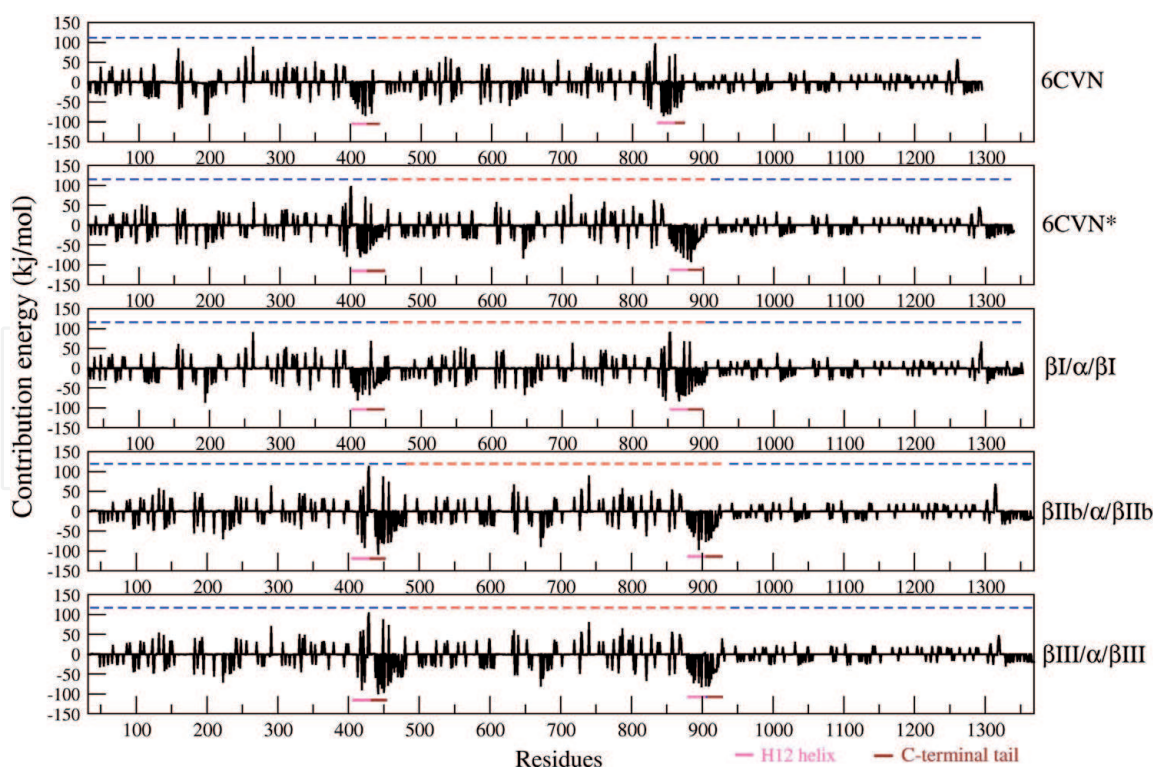


Figure 13.

The H12 and C-terminal tail regions show highest energy contribution for the binding of TauR2 in 6CVN*, $\beta I/\alpha/\beta I$, $\beta IIb/\alpha/\beta IIb$ and $\beta III/\alpha/\beta III$ tubulin subunits except in case of 6CVN which does not have C-terminal tail region.

shows maximum contribution in the binding energy (**Figure 13**). The per-residue interactions energy (residue decomposition energy) calculated for various pairs of interacting residues highlights the importance of the interacting residues. The residues from the H12-helices and C-terminal tail region of complex $\beta III/\alpha/\beta III$ shows maximum contribution (most negative energy) in the non-bonded contacts leading to the stable and tight binding of the tauR2 to the $\beta III/\alpha/\beta III$ tubulin subunits.

Hence, relative binding energy calculations further support all other MD simulation results highlighting the tight binding of TauR2 to the $\beta III/\alpha/\beta III$ tubulin isotype which is predominantly expressed in the neuronal cells and brain.

4. Conclusion

MTs are distributed across all types of cells and play an important role in the cellular functions. Structurally MTs are made up of α/β heterodimeric subunits. Large diversity of α and β -tubulin isotypes exists which are differently expressed in different types of cells, this makes MTs unique from one another in relative proportion of isotypes. The much elevated expression levels of βII and βIII tubulin isotypes about 58% and 25% respectively have been reported to in neuronal cells and brain [35]. The present study extensively uses molecular modeling approaches including homology modeling, MD simulation, binding energy to investigate the binding mode and interaction of neuronal specific tubulin isotypes with TauR2.

Extensive analysis on MD simulation trajectory shows a stable complex formation in between different tubulin isotype and TauR2. The stability of these complexes is mainly mediated by the interactions of H12 helix and C-terminal tail of the α/β tubulin isotypes with TauR2. TauR2 shows differential binding affinity towards various neuronal specific β -tubulin isotypes (βI , βII and βIII) the order of binding affinity is ' $\beta III > \beta IIb > \beta I$ '. Thus, it is found that TauR2 expresses greater binding affinity with βIII

and β IIb tubulin isoforms which are abundantly expressed in neuronal cells and brain. The molecular modeling strategy adopted in this chapter could be potentially used to understand differential binding affinity of other tau repeats such as R1, R3, R4 towards β tubulin isoforms present in other cell lines. The structures for other repeats could be generated using homology modeling and their interactions with neuronal specific tubulin isoforms could also be studied using similar molecular modeling approach. I believe that the knowledge on precise molecular origin of differential binding affinity of tau with β tubulin isoforms present different cell types will pave the way for developing effective treatments against tau related disorders such as Alzheimers, Amyotrophic lateral sclerosis and other tauopathy linked neurodegenerative disorders.

Thus, homology modeling allows us to investigate important biomolecular interactions whose protein structures are not known and/or difficult to get by using biophysical experiments. This, homology modeling, computational tool has made it easier to address various challenging problems in understanding the basic phenomenon's/pathways in modern biology. Also, it has proven wide successful applications in determining the role of proteins in various genetic diseases, hormonal disorder cancers, neurological disorders and other diseases etc. by exploring protein structure and functions using molecular modeling techniques.

Acknowledgements

VVB is thankful to IIT Bombay for Institute postdoctoral fellowship. Author is also thankful to Prof. Ambarish Kunwar, Department of Biosciences and Bioengineering, IIT Bombay, Mumbai for fruitful discussion and providing necessary computational resources to perform this research work. Author also sincerely thanks Creative Commons license for giving permission to use data from my manuscript my published research article in Scientific Reports (<https://doi.org/10.1038/s41598-019-47249-7>). A copy of creative commons license can be found at the link <http://creativecommons.org/licenses/by/4.0/>

Conflict of interest

The author declares no conflict of interest.

Author details

Vishwambhar Vishnu Bhandare
Department of Biosciences and Bioengineering, Indian Institute of Technology
Bombay, Mumbai, India

*Address all correspondence to: vishwayogi@gmail.com

IntechOpen

© 2021 The Author(s). Licensee IntechOpen. This chapter is distributed under the terms of the Creative Commons Attribution License (<http://creativecommons.org/licenses/by/3.0/>), which permits unrestricted use, distribution, and reproduction in any medium, provided the original work is properly cited. 

References

- [1] Bayat A. Science, medicine, and the future: Bioinformatics. *BMJ* [Internet]. 2002;324(7344):1018-22. Available from: <http://www.ncbi.nlm.nih.gov/pubmed/11976246>
- [2] Melo AM, Coraor J, Alpha-Cobb G, Elbaum-Garfinkle S, Nath A, Rhoades E. A functional role for intrinsic disorder in the tau-tubulin complex. *Proc Natl Acad Sci* [Internet]. 2016;113(50):14336-41. Available from: <http://www.pnas.org/lookup/doi/10.1073/pnas.1610137113>
- [3] Butner KA, Kirschner MW. Tau Protein Binds to Microtubules through. *J Cell Biol.* 1991;115(3):717-30.
- [4] Guo T, Noble W, Hanger DP. Roles of tau protein in health and disease. *Acta Neuropathol* [Internet]. 2017 May;133(5):665-704. Available from: <http://www.ncbi.nlm.nih.gov/pubmed/28386764>
- [5] Liu F, Gong C-X. Tau exon 10 alternative splicing and tauopathies. *Mol Neurodegener* [Internet]. 2008;3(1):8. Available from: <http://molecularneurodegeneration.biomedcentral.com/articles/10.1186/1750-1326-3-8>
- [6] Buée L, Bussièrè T, Buée-Scherrer V, Delacourte A, Hof PR. Tau protein isoforms, phosphorylation and role in neurodegenerative disorders. *Brain Res Rev.* 2000;33(1):95-130.
- [7] Kolarova M, García-Sierra F, Bartos A, Ricny J, Ripova D. Structure and Pathology of Tau Protein in Alzheimer Disease. *Int J Alzheimers Dis* [Internet]. 2012;2012:1-13. Available from: <http://www.hindawi.com/journals/ijad/2012/731526/>
- [8] Kellogg EH, Hejab NMA, Poepsel S, Downing KH, DiMaio F, Nogales E. Near-atomic model of microtubule-tau interactions. *Science* (80-) [Internet]. 2018;1780(May):eaat1780. Available from: <http://www.sciencemag.org/lookup/doi/10.1126/science.aat1780>
- [9] Jebarupa B, Muralidharan M, Arun A, Mandal AK, Mitra G. Conformational heterogeneity of tau: Implication on intrinsic disorder, acid stability and fibrillation in Alzheimer's disease. *Biophys Chem* [Internet]. 2018 Oct;241:27-37. Available from: <http://www.ncbi.nlm.nih.gov/pubmed/30081240>
- [10] Qiang L, Sun X, Austin TO, Muralidharan H, Jean DC, Liu M, et al. Tau Does Not Stabilize Axonal Microtubules but Rather Enables Them to Have Long Labile Domains. *Curr Biol* [Internet]. 2018 Jul 9;28(13):2181-2189.e4. Available from: <http://www.ncbi.nlm.nih.gov/pubmed/30008334>
- [11] Brettschneider J, Arai K, Del Tredici K, Toledo JB, Robinson JL, Lee EB, et al. TDP-43 pathology and neuronal loss in amyotrophic lateral sclerosis spinal cord. *Acta Neuropathol.* 2014;128(3):423-437.
- [12] Gao Y-L, Wang N, Sun F-R, Cao X-P, Zhang W, Yu J-T. Tau in neurodegenerative disease. *Ann Transl Med* [Internet]. 2018 May;6(10):175-175. Available from: <http://atm.amegroups.com/article/view/19456/19578>
- [13] Friedhoff P, von Bergen M, Mandelkow E-M, Mandelkow E. Structure of tau protein and assembly into paired helical filaments. *Biochim Biophys Acta - Mol Basis Dis* [Internet]. 2000;1502(1):122-32. Available from: <http://linkinghub.elsevier.com/retrieve/pii/S0925443900000387>
- [14] Kellogg EH, Hejab NMA, Poepsel S, Downing KH, DiMaio F, Nogales E. Near-atomic model of microtubule-tau

- interactions. *Science* (80-) [Internet]. 2018;eaat1780. Available from: <http://www.sciencemag.org/lookup/doi/10.1126/science.aat1780>
- [15] Kadavath H, Cabrales Fontela Y, Jaremko M, Jaremko Ł, Overkamp K, Biernat J, et al. The Binding Mode of a Tau Peptide with Tubulin. *Angew Chemie Int Ed* [Internet]. 2018 Mar 12;57(12):3246-50. Available from: <http://doi.wiley.com/10.1002/anie.201712089>
- [16] Panda D, Samuel JC, Massie M, Feinstein SC, Wilson L. Differential regulation of microtubule dynamics by three- and four-repeat tau: Implications for the onset of neurodegenerative disease. *Proc Natl Acad Sci* [Internet]. 2003 Aug 5;100(16):9548-53. Available from: <http://www.pnas.org/cgi/doi/10.1073/pnas.1633508100>
- [17] Panda D, Goode BL, Feinstein SC, Wilson L. Kinetic Stabilization of Microtubule Dynamics at Steady State by Tau and Microtubule-Binding Domains of Tau. *Biochemistry* [Internet]. 1995 Sep 5;34(35):11117-27. Available from: <http://pubs.acs.org/doi/abs/10.1021/bi00035a017>
- [18] Ludueña RF. A Hypothesis on the Origin and Evolution of Tubulin [Internet]. Vol. 302, *International Review of Cell and Molecular Biology*. Elsevier; 2013. 41-185 p. Available from: <http://dx.doi.org/10.1016/B978-0-12-407699-0.00002-9>
- [19] Ludueña RF, Banerjee A. The Isoforms of Tubulin. In: *The Role of Microtubules in Cell Biology, Neurobiology, and Oncology* [Internet]. Totowa, NJ: Humana Press; 2008. p. 123-75. Available from: http://link.springer.com/10.1007/978-1-59745-336-3_6
- [20] Guo J, Walss-Bass C, Ludueña RF. The beta isoforms of tubulin in neuronal differentiation. *Cytoskeleton* (Hoboken) [Internet]. 2010 Jul;67(7):431-41. Available from: <http://www.ncbi.nlm.nih.gov/pubmed/20506160>
- [21] Kumbhar BV, Borogaon A, Panda D, Kunwar A. Exploring the Origin of Differential Binding Affinities of Human Tubulin Isoforms $\alpha\beta$ II, $\alpha\beta$ III and $\alpha\beta$ IV for DAMA-Colchicine Using Homology Modelling, Molecular Docking and Molecular Dynamics Simulations. Toda T, editor. *PLoS One* [Internet]. 2016 May 26;11(5):e0156048. Available from: <https://dx.plos.org/10.1371/journal.pone.0156048>
- [22] Kumbhar BV, Panda D, Kunwar A. Interaction of microtubule depolymerizing agent indanocine with different human $\alpha\beta$ tubulin isoforms. 2018;1-20. Available from: <http://journals.plos.org/plosone/article/file?id=10.1371/journal.pone.0194934&type=printable>
- [23] Pamula MC, Ti S-C, Kapoor TM. The structured core of human β tubulin confers isoform-specific polymerization properties. *J Cell Biol* [Internet]. 2016 May 23;213(4):425-33. Available from: <http://www.jcb.org/lookup/doi/10.1083/jcb.201603050>
- [24] Fees CP, Aiken J, O'Toole ET, Giddings TH, Moore JK. The negatively charged carboxy-terminal tail of β -tubulin promotes proper chromosome segregation. *Mol Biol Cell* [Internet]. 2016;27(11):1786-96. Available from: <http://www.molbiolcell.org/lookup/doi/10.1091/mbc.E15-05-0300>
- [25] Roll-Mecak A. Intrinsically disordered tubulin tails: complex tuners of microtubule functions? *Semin Cell Dev Biol* [Internet]. 2015 Jan;37:11-9. Available from: <http://www.ncbi.nlm.nih.gov/pubmed/25307498>
- [26] Janke C. The tubulin code: Molecular components, readout mechanisms, functions. *J Cell Biol*. 2014;206(4):461-72.

- [27] Pamula MC, Ti S-C, Kapoor TM. The structured core of human β tubulin confers isotype-specific polymerization properties. *J Cell Biol* [Internet]. 2016;213(4):425-33. Available from: <http://www.ncbi.nlm.nih.gov/pubmed/27185835>
- [28] Panda D, Miller HP, Banerjee A, Luduena RF, Wilson L. Microtubule dynamics in vitro are regulated by the tubulin isotype composition. *Proc Natl Acad Sci* [Internet]. 1994 Nov 22;91(24):11358-62. Available from: <http://www.ncbi.nlm.nih.gov/pubmed/7972064>
- [29] Shojania Feizabadi M, Janakaloti Narayanareddy BR, Vadpey O, Jun Y, Chapman D, Rosenfeld S, et al. Microtubule C-Terminal Tails Can Change Characteristics of Motor Force Production. *Traffic* [Internet]. 2015 Oct;16(10):1075-87. Available from: <http://doi.wiley.com/10.1111/tra.12307>
- [30] Banerjee A, Luduena RF. Kinetics of colchicine binding to purified beta-tubulin isotypes from bovine brain. *J Biol Chem*. 1992;267(19):13335-9.
- [31] Cowan NJ, Lewis SA, Gu W, Buraoyne RD. Tubulin Isotypes and Their Interaction with Microtubule Associated Proteins. *Protoplasma*. 1988;145:6-111.
- [32] Murphy DB. Purification of Tubulin and Tau from Chicken Erythrocytes: Tubulin Isotypes and Mechanisms of Microtubule Assembly. *Methods Enzymol*. 1991;196(1986):235-46.
- [33] Ludueuna RF. Are Tubulin Isotypes Functionally Significant. *Mol Biol Cell*. 1993;4(May):445-57.
- [34] Vemu A, Atherton J, Spector JO, Moores CA, Roll-Mecak A. Tubulin isoform composition tunes microtubule dynamics. *Mol Biol Cell* [Internet]. 2017 Dec 1;28(25):3564-72. Available from: <http://www.ncbi.nlm.nih.gov/pubmed/29021343>
- [35] Feizabadi MS, Hernandez MAV, Breslin JB, Akintola II. The regulatory effect of Tau protein on polymerization of MCF7 microtubules in vitro. *Biochem Biophys Reports* [Internet]. 2019 Mar;17:151-6. Available from: <https://linkinghub.elsevier.com/retrieve/pii/S2405580818302528>
- [36] Bhandare VV, Kumbhar BV, Kunwar A. Differential binding affinity of tau repeat region R2 with neuronal-specific β -tubulin isotypes. *Sci Rep* [Internet]. 2019 Jul 25;9(1):10795. Available from: <http://www.ncbi.nlm.nih.gov/pubmed/31346240>
- [37] Sievers F, Wilm A, Dineen D, Gibson TJ, Karplus K, Li W, et al. Fast, scalable generation of high-quality protein multiple sequence alignments using Clustal Omega. *Mol Syst Biol* [Internet]. 2014 Apr 16;7(1):539-539. Available from: <http://msb.embopress.org/cgi/doi/10.1038/msb.2011.75>
- [38] Webb B, Sali A. Comparative Protein Structure Modeling Using MODELLER. In: *Current Protocols in Bioinformatics* [Internet]. Hoboken, NJ, USA: John Wiley & Sons, Inc.; 2016. p. 5.6.1-5.6.37. Available from: <http://doi.wiley.com/10.1002/cpbi.3>
- [39] Biasini M, Bienert S, Waterhouse A, Arnold K, Studer G, Schmidt T, et al. SWISS-MODEL: modelling protein tertiary and quaternary structure using evolutionary information. *Nucleic Acids Res* [Internet]. 2014 Jul 1;42(W1):W252-8. Available from: <http://academic.oup.com/nar/article/42/W1/W252/2435313/SWISSMODEL-modelling-protein-tertiary-and>
- [40] Eisenberg D, Lüthy R, Bowie JU. [20] VERIFY3D: Assessment of protein models with three-dimensional profiles. *Methods Enzymol*. 1997;277:396-404.
- [41] Colovos C, Yeates TO. Verification of protein structures: patterns of nonbonded atomic interactions. *Protein*

- Sci [Internet]. 1993 Sep;2(9):1511-9. Available from: <http://www.ncbi.nlm.nih.gov/pubmed/8401235>
- [42] Laskowski RA, MacArthur MW, Moss DS, Thornton JM. PROCHECK: a program to check the stereochemical quality of protein structures. *J Appl Crystallogr* [Internet]. 1993 Apr 1;26(2):283-91. Available from: <http://scripts.iucr.org/cgi-bin/paper?S0021889892009944>
- [43] Van Der Spoel D, Lindahl E, Hess B, Groenhof G, Mark AE, Berendsen HJC. GROMACS: fast, flexible, and free. *J Comput Chem*. 2005;26(16):1701-1718.
- [44] Karplus M, McCammon JA. Molecular dynamics simulations of biomolecules. *Nat Struct Mol Biol*. 2002;9(9):646-52.
- [45] Hospital A, Goñi JR, Orozco M, Gelpí JL. Molecular dynamics simulations: advances and applications. *Adv Appl Bioinforma Chem AABC*. 2015;10:37.
- [46] Berendsen HJC, van der Spoel D, van Drunen R. GROMACS: A message-passing parallel molecular dynamics implementation. *Comput Phys Commun*. 1995;91(1-3):43-56.
- [47] Lindorff-Larsen K, Piana S, Palmo K, Maragakis P, Klepeis JL, Dror RO, et al. Improved side-chain torsion potentials for the Amber ff99SB protein force field. *Proteins Struct Funct Bioinforma* [Internet]. 2010;78(8):NA-NA. Available from: <http://doi.wiley.com/10.1002/prot.22711>
- [48] Meagher KL, Redman LT, Carlson HA. Development of polyphosphate parameters for use with the AMBER force field. *J Comput Chem* [Internet]. 2003 Jul 15;24(9):1016-25. Available from: <http://www.ncbi.nlm.nih.gov/pubmed/12759902>
- [49] Allnér O, Nilsson L, Villa A. Magnesium Ion-Water Coordination and Exchange in Biomolecular Simulations. *J Chem Theory Comput* [Internet]. 2012 Apr 10;8(4):1493-502. Available from: <http://www.ncbi.nlm.nih.gov/pubmed/26596759>
- [50] Case DA, Darden TA, Cheatham III TE, Simmerling CL, Wang J, Duke RE, et al. AMBER 12; University of California: San Francisco, 2012. 2012;
- [51] ParmEd tool [Internet]. Available from: <http://parmed.github.io/ParmEd/html/index.html>
- [52] Bhandare VV, Ramaswamy A. The proteinopathy of D169G and K263E mutants at the RNA Recognition Motif (RRM) domain of tar DNA-binding protein (tdp43) causing neurological disorders: A computational study. *J Biomol Struct Dyn*. 2017;
- [53] Essmann U, Perera L, Berkowitz ML, Darden T, Lee H, Pedersen LG. A smooth particle mesh Ewald method. *J Chem Phys* [Internet]. 1995 Nov 15;103(19):8577-93. Available from: <http://aip.scitation.org/doi/10.1063/1.470117>
- [54] Darden T, York D, Pedersen L. Particle mesh Ewald: An $N \cdot \log(N)$ method for Ewald sums in large systems. *J Chem Phys* [Internet]. 1993 Jun 15;98(12):10089-92. Available from: <http://aip.scitation.org/doi/10.1063/1.464397>
- [55] Hess B, Bekker H, Berendsen HJC, Fraaije JG. LINCS: A Linear Constraint Solver for Molecular Simulations. *Artic / Lett to Ed*. 1977;18:1463-1472.
- [56] Kabsch W, Sander C. Dictionary of protein secondary structure: pattern recognition of hydrogen-bonded and geometrical features. *Biopolymers* [Internet]. 1983/12/01. 1983;22(12):2577-637. Available from: http://www.ncbi.nlm.nih.gov/entrez/query.fcgi?cmd=Retrieve&db=PubMed&dopt=Citation&list_uids=6667333

- [57] Humphrey W, Dalke A, Schulten K. VMD: visual molecular dynamics. *J Mol Graph* [Internet]. 1996/02/01. 1996;14(1):27-28,33-38. Available from: http://www.ncbi.nlm.nih.gov/entrez/query.fcgi?cmd=Retrieve&db=PubMed&dopt=Citation&list_uids=8744570
- [58] Biovia Discovery studio Visualizer. Daasault Systemes BIOVIA; 2017.
- [59] Pettersen EF, Goddard TD, Huang CC, Couch GS, Greenblatt DM, Meng EC, et al. UCSF Chimera--a visualization system for exploratory research and analysis. *J Comput Chem*. 2004;25(13):1605-1612.
- [60] Hess B, van Der Spoel D, Lindahl E. *Gromacs user manual version 4.5*. 4. Univ Groningen, Netherl. 2010;
- [61] Gilson MK, Zhou HX. Calculation of protein-ligand binding affinities. *Annu Rev Biophys Biomol Struct* [Internet]. 2007;36:21-42. Available from: <http://www.ncbi.nlm.nih.gov/pubmed/17201676>
- [62] Genheden S, Ryde U. The MM/PBSA and MM/GBSA methods to estimate ligand-binding affinities. *Expert Opin Drug Discov* [Internet]. 2015;10(5):449-61. Available from: <http://www.ncbi.nlm.nih.gov/pubmed/25835573>
- [63] Wong S, Amaro RE, McCammon JA. MM-PBSA Captures Key Role of Intercalating Water Molecules at a Protein-Protein Interface. *J Chem Theory Comput* [Internet]. 2009 Feb 10;5(2):422-9. Available from: <http://pubs.acs.org/doi/abs/10.1021/ct8003707>
- [64] Aldeghi M, Bodkin MJ, Knapp S, Biggin PC. Statistical Analysis on the Performance of Molecular Mechanics Poisson-Boltzmann Surface Area versus Absolute Binding Free Energy Calculations: Bromodomains as a Case Study. *J Chem Inf Model* [Internet]. 2017 Sep 25;57(9):2203-21. Available from: <http://pubs.acs.org/doi/10.1021/acs.jcim.7b00347>
- [65] Kant V, Vijayakumar S, Sahoo GC, Chaudhery SS, Das P. In-silico screening and validation of high-affinity tetrapeptide inhibitor of Leishmania donovani O-acetyl serine sulfhydrylase (OASS). *J Biomol Struct Dyn* [Internet]. 2018 Feb 7;1-14. Available from: <https://www.tandfonline.com/doi/full/10.1080/07391102.2018.1429315>
- [66] Paissoni C, Spiliotopoulos D, Musco G, Spitaleri A. GMXPBSA 2.0: A GROMACS tool to perform MM/PBSA and computational alanine scanning. *Comput Phys Commun*. 2014;185(11):2920-9.
- [67] Bhandare VV, Ramaswamy A. Structural dynamics of human argonaute2 and its interaction with siRNAs designed to target mutant tdp43. *Adv Bioinformatics*. 2016;2016.
- [68] Kumari R, Kumar R, Lynn A. g_mmpbsa-A GROMACS Tool for High-Throughput MM-PBSA Calculations. *J Chem Inf Model*. 2014;54(7):1951-1962.
- [69] Cavuturu BM, Bhandare VV, Ramaswamy A, Arumugam N. Molecular dynamics of interaction of Sesamin and related compounds with the cancer marker β -catenin: an in silico study. *J Biomol Struct Dyn*. 2018;
- [70] Guo W, Chen Y, Zhou X, Kar A, Ray P, Chen X, et al. An ALS-associated mutation affecting TDP-43 enhances protein aggregation, fibril formation and neurotoxicity. *Nat Struct Mol Biol* [Internet]. 2011/06/15. 18(7):822-30. Available from: http://www.ncbi.nlm.nih.gov/entrez/query.fcgi?cmd=Retrieve&db=PubMed&dopt=Citation&list_uids=21666678
- [71] Wang C, Greene D, Xiao L, Qi R, Luo R. Recent Developments and

Applications of the MMPBSA Method. *Front Mol Biosci* [Internet]. 2017;4:87. Available from: <http://www.ncbi.nlm.nih.gov/pubmed/29367919>

[72] Miller BR, McGee TD, Swails JM, Homeyer N, Gohlke H, Roitberg AE. MMPBSA.py: An Efficient Program for End-State Free Energy Calculations. *J Chem Theory Comput* [Internet]. 2012 Sep 11;8(9):3314-21. Available from: <http://www.ncbi.nlm.nih.gov/pubmed/26605738>

[73] Ti S-C, Alushin GM, Kapoor TM. Human β -Tubulin Isoforms Can Regulate Microtubule Protofilament Number and Stability. *Dev Cell* [Internet]. 2018 Sep; Available from: <https://linkinghub.elsevier.com/retrieve/pii/S1534580718306841>

[74] Biasini M, Bienert S, Waterhouse A, Arnold K, Studer G, Schmidt T, et al. SWISS-MODEL: Modelling protein tertiary and quaternary structure using evolutionary information. *Nucleic Acids Res*. 2014;42(W1).

[75] Wiederstein M, Sippl MJ. ProSA-web: interactive web service for the recognition of errors in three-dimensional structures of proteins. *Nucleic Acids Res* [Internet]. 2007 Jul;35(Web Server issue):W407-10. Available from: <http://www.ncbi.nlm.nih.gov/pubmed/17517781>

[76] Lovell SC, Davis IW, Arendall WB, de Bakker PIW, Word JM, Prisant MG, et al. Structure validation by Calpha geometry: phi, psi and Cbeta deviation. *Proteins* [Internet]. 2003 Feb 15;50(3):437-50. Available from: <http://www.ncbi.nlm.nih.gov/pubmed/12557186>

[77] RAMACHANDRAN GN, RAMAKRISHNAN C, SASISEKHARAN V. Stereochemistry of polypeptide chain configurations. *J Mol Biol* [Internet]. 1963 Jul;7:95-9. Available

from: <http://www.ncbi.nlm.nih.gov/pubmed/13990617>

[78] Van Der Spoel D, Lindahl E, Hess B, Groenhof G, Mark AE, Berendsen HJ. GROMACS: fast, flexible, and free. *J Comput Chem* [Internet]. 2005/10/08. 2005;26(16):1701-18. Available from: http://www.ncbi.nlm.nih.gov/entrez/query.fcgi?cmd=Retrieve&db=PubMed&dopt=Citation&list_uids=16211538

[79] Kar S, Fan J, Smith MJ, Goedert M, Amos LA. Repeat motifs of tau bind to the insides of microtubules in the absence of taxol. *EMBO J* [Internet]. 2003 Jan 2;22(1):70-7. Available from: <http://www.ncbi.nlm.nih.gov/pubmed/12505985>

[80] Chau M-F, Radeke MJ, de Inés C, Barasoain I, Kohlstaedt LA, Feinstein SC. The Microtubule-Associated Protein Tau Cross-Links to Two Distinct Sites on Each α and β Tubulin Monomer via Separate Domains †. *Biochemistry* [Internet]. 1998 Dec;37(51):17692-703. Available from: <http://pubs.acs.org/doi/abs/10.1021/bi9812118>

[81] Al-Bassam J, Ozer RS, Safer D, Halpain S, Milligan RA. MAP2 and tau bind longitudinally along the outer ridges of microtubule protofilaments. *J Cell Biol*. 2002;157(7):1187-96.

[82] Santarella RA, Skiniotis G, Goldie KN, Tittmann P, Gross H, Mandelkow E-M, et al. Surface-decoration of microtubules by human tau. *J Mol Biol* [Internet]. 2004 Jun 4;339(3):539-53. Available from: <http://www.ncbi.nlm.nih.gov/pubmed/15147841>

[83] Luo Y, Ma B, Nussinov R, Wei G. Structural Insight into Tau Protein's Paradox of Intrinsically Disordered Behavior, Self-Acetylation Activity, and Aggregation. *J Phys Chem Lett* [Internet]. 2014 Sep 4;5(17):3026-31. Available from: <http://www.ncbi.nlm.nih.gov/pubmed/25206938>

[84] Avila J, Jiménez JS, Sayas CL, Bolós M, Zabala JC, Rivas G, et al. Tau Structures. *Front Aging Neurosci* [Internet]. 2016;8:262. Available from: <http://www.ncbi.nlm.nih.gov/pubmed/27877124>

[85] Fischer D, Mukrasch MD, Von Bergen M, Klos-Witkowska A, Biemat J, Griesinger C, et al. Structural and microtubule binding properties of tau mutants of frontotemporal dementias. *Biochemistry*. 2007;46(10):2574-82.

[86] Ma B, Wei G, Zhen J, Nussinov R. Dancing with Strings: The Conformational Dynamics of VQIXXK Motifs within Tau Protein in Monomer, Fibril and Hyper-Phosphorylated Filament States. *Biophys J* [Internet]. 2016;110(3):553a-554a. Available from: <http://linkinghub.elsevier.com/retrieve/pii/S0006349515041430>